Design of lean duplex stainless steel tubular sections subjected to concentrated end-bearing loads

Yancheng Cai, M.ASCE[1] and Ben Young, F.ASCE[2]

ABSTRACT

This paper presents the numerical investigation and design of cold-formed lean duplex stainless steel (CFLDSS) tubular sections subjected to concentrated end bearing loads. i.e., the loading conditions of End-One-Flange (EOF), End-Two-Flange (ETF) and end loading (EL). Finite element models (FEMs) were developed and verified against the test results of CFLDSS tubular sections subjected to the three concentrated end bearing loads. It is shown that the FEMs are able to predict the behaviour of CFLDSS tubular sections subjected to the three concentrated end bearing loads in terms of ultimate strengths and web crippling failure. Hence, the verified FEMs were used to perform an extensive parametric study that covered the key parameters in a wide range, including the ratios of flat web height to thickness, load bearing length to web thickness and load bearing length to flat web height. Based on both the test and numerical results, new coefficients are proposed for the unified design equation in North American Specification (NAS) and the direct strength method (DSM) for design of CFLDSS tubular sections subjected to the three concentrated end bearing loads. The strengths obtained from the tests and parametric study were compared with the nominal strengths calculated using the design equations from the current specifications of ASCE, Australian/New Zealand (AS/NZS), NAS and Eurocode (EC3), and those in the literature, as well as the modified design rules proposed in this study. Overall, it is shown that the modified design rules provided more accurate predictions compared with the design rules in current specifications and literature. The results showed that the proposed design

[1] Research Assistant Professor, Department of Civil and Environmental Engineering, The Hong Kong Polytechnic University, Hong Kong. (corresponding author). E-mail: yancheng.cai@polyu.edu.hk
(Formerly, Dept. of Civil Engineering, Univ. of Hong Kong, Pokfulam Rd., Hong Kong.)
[2] Professor, Department of Civil and Environmental Engineering, The Hong Kong Polytechnic University, Hong Kong. E-mail: ben.young@polyu.edu.hk (Formerly, Dept. of Civil Engineering, Univ. of Hong Kong, Pokfulam Rd., Hong Kong.)

methods are suitable for the web crippling design of CFLDSS tubular sections under the three concentrated end bearing loads.

Keywords*:* Design rules, direct strength method, lean duplex stainless steel, numerical investigation, concentrated bearing loads, web crippling.

INTRODUCTION

Webs of steel tubular members may cripple under high concentrated bearing loads (Zhou and Young 2007a), for examples, thin-walled steel square and rectangular tubular members with slender webs. Hence, web crippling strengths of these tubular members should be checked carefully under the condition of concentrated bearing loads. The computation of the web crippling strength by means of theoretical analysis is quite complex (Young and Hancock 2001). The current design rules in most specifications for web crippling of steel tubular members are empirical in nature.

Stainless steel is more expensive than carbon steel, however, stainless steel structures as compared with carbon steel structures are superior in appearance, corrosion resistance and fire resistance, as well as lower in life cycle costs (Gardner and Baddoo 2006), these may counterbalance the initial higher cost of the stainless steel materials. Investigations on the web crippling strengths of stainless steel members have been conducted. These covered different grades of stainless steel, including austenitic stainless steel (dos Santos et al 2018; dos Santos and Gardner 2019; Gardner et al. 2006; Zhou and Young 2006), ferritic stainless steel (Bock et al 2013; Li and Young 2017; Li and Young 2018), duplex stainless steel (Zhou and Young 2007a; Zhou and Young 2007b), and lean duplex stainless steel (Cai and Young 2019a; Cai and Young 2019b). Different conditions of concentrated bearing load were considered in these investigations, including the loading conditions of End-One-Flange (EOF) (Bock et al 2013; Cai and Young 2019a; dos Santos and Gardner 2019; Li and Young 2018; Zhou and Young 2007b), Interior-One-Flange (IOF) (Bock et al 2013; Cai and Young 2019b; dos Santos et al 2018;

Gardner et al. 2006; Li and Young 2018; Zhou and Young 2007b;), End-Two-Flange (ETF) (Cai and Young 2019a; Li and Young 2018; Zhou and Young 2006; Zhou and Young 2007b;) and Interior-Two-Flange (ITF) (Cai and Young 2019b; dos Santos et al 2018; Li and Young 2018; Zhou and Young 2006; Zhou and Young 2007b;) as well as the end loading (EL) (Cai and Young 2019a; Li and Young 2017; Zhou and Young 2007a) and interior loading (IL) (Cai and Young 2019b; Li and Young 2017; Zhou and Young 2007a). Nonetheless, it should be noted that the design rules in the current international stainless steel specifications (ASCE 2002; AS/NZS 2001; EC3-1.4 2015) for web crippling strengths of stainless steel members are mainly adopted from those of carbon steel members, i.e., the American Society of Civil Engineers (ASCE) Specification (ASCE 2002), the Australian/ New Zealand Standard (AS/NZS 2001) and the European Code (EC3-1.4 2015).

The relatively new stainless steel material, lean duplex stainless steel, has gained significant attention in construction industry recently. The lean duplex stainless steel material is much cheaper than the conventional austenitic stainless steel due to the significant reduction in the nickel content, i.e., around 1.5% compared with 8~10% (Huang and Young 2012). The nickel represents a significant portion of material cost in stainless steel. The lean duplex type still offers higher yield strength and comparable corrosion resistance compared to the austenitic type. A wide range of investigations have been carried out for the structural behaviour of lean duplex stainless steel. These investigations included the material properties (Huang and Young 2012; Saliba and Gardner 2013a; Theofanous and Gardner 2009; Theofanous and Gardner 2010), beams (Huang and Young 2014; Saliba and Gardner 2013a; Theofanous and Gardner 2010; Zhao et al 2017; Zhao and Gardner 2018) and columns (Huang and Young 2013; Zhao et al 2015a; Zhao et al 2015b), plate girders (Saliba and Gardner 2013b; Saliba et al 2014), single shear bolted connections (Cai and Young 2014a; Cai and Young 2014b; Cai and Young 2014c) and double shear bolted connections (Cai and Young 2014a; Cai and Young 2015). These research outcomes lead to the significant development in the design of lean duplex stainless steel structures. However, it should be noted that the lean duplex stainless steel is not covered in the current

74 ASCE (2002) and AS/NZS (2001) specifications, while it was recently introduced in the EC3-1.4
75 (2015).

76 Up-to-date, limited research works on the web crippling behaviour of lean duplex stainless steel
77 sections have been conducted. Recent experimental investigations of over 100 cold-formed lean duplex
78 stainless steel (CFLDSS) tubular members undergoing web crippling were carried out by Cai and
79 Young (2019a; 2019b). They showed that the strengths predicted by the current stainless steel (ASCE
80 2002; AS/NZS 2001; EC3-1.4 2015) and carbon steel (2016) design specifications, as well as the
81 design rules in the literature (Zhou and Young 2008) were generally conservative.

82 In this paper, numerical investigation and design of CFLDSS tubular sections under concentrated end
83 bearing loads, i.e., the loading conditions of EOF, ETF and EL, are presented. Finite element models
84 (FEMs) were developed and verified against the test results of CFLDSS tubular sections under the
85 loading conditions of EOF, ETF and EL in terms of ultimate strengths (web crippling strengths) and
86 failure modes. The verified FEMs were employed to perform an extensive parametric study that
87 consisted of 144 CFLDSS tubular sections. The sections in the parametric study were designed to
88 cover a wide range of key parameters, including the ratios of flat web height to thickness, load bearing
89 length to web thickness and load bearing length to flat web height. The test and numerical strengths of
90 the specimens were compared with the nominal strengths predicted by the current design specifications
91 of stainless steel (ASCE 2002; AS/NZS 2001 and EC-1.4 2015) and carbon steel (NAS (2016)), as
92 well as by the design rules in the literature (Li and Young 2017; Li and Young 2018; Zhou and Young
93 2008). Note that EC3-1.4 (2015) does not have specific design rules for web crippling of stainless
94 steel sections and may refer to those specified in the EC3-1.3 (2006). New coefficients are proposed
95 for the unified design equation specified in the NAS (2016) and the direct strength method (DSM) (Li
96 and Young 2017; Li and Young 2018) for the web crippling design of CFLDSS tubular sections under
97 the loading conditions of EOF, ETF and EL. Reliability analysis was conducted for the current and
98 modified design rules.

SUMMARY OF EXPERIMENTAL INVESTIGATION

The test program of CFLDSS tubular sections subjected to concentrated end bearing loads conducted by Cai and Young (2019a) provided the experimental ultimate strengths, load-deformation curves and web crippling failure modes of the sections. The three different concentrated end bearing loads were considered in the test program, namely, the EOF, ETF and EL. The EOF and ETF loading conditions are specified in the ASCE (2002) and AS/NZS (2001) stainless steel design specifications, while the EL condition simulated the floor joist members positioned on a solid foundation under concentrated end bearing load.

The test specimens were fabricated from two different grades of CFLDSS, i.e., the EN 1.4062 (AISI S32202) and EN 1.4162 (AISI S32101). Tensile and compressive coupon tests were conducted to obtain the material properties. The tensile coupons were extracted in the longitudinal direction of the sections, whereas the compressive coupons were extracted in the transverse direction of the webs. The coupon dimensions and test results are detailed in Cai and Young (2019a). Table 1 shows the Young's modulus (E_T and E_C), 0.2% proof stress ($f_{0.2,T}$ and $f_{0.2,C}$) and strain at fracture ($\varepsilon_{f,T}$) of the CFLDSS tubular members, where the subscripts "*T*" and "*C*" represent the results obtained from tensile and compressive coupons, respectively.

Figure 1 illustrates the definition of the symbols in a CFLDSS section, where H and h are the over height and the flat portion of the section web, respectively; B is the width of the section; t is the section thickness and r_i is the section inner radius. Totally fifty CFLDSS specimens were tested under concentrated end bearing loads (Cai and Young 2019a). These covered nine square and rectangular hollow sections ($H\times B\times t$). They are sections of 20×50×1.5, 40×60×2.0, 50×20×1.5, 60×40×2.0, 60×120×3.0, 80×150×3.0, 100×100×3.0, 120×60×3.0 and 150×80×3.0 in the unit of mm. The variation of parameters included the three concentrated end loading conditions (EOF, ETF and EL), six bearing lengths (N) of steel loading plate and a range of web slenderness ratio h/t and the ratios of inner corner radius (r_i) to tube thickness. It should be noted that flanges fastened or non-fastened to

the supports were provided in the web crippling design of specifications (ASCE 2002; AS/NZS 2001; EC3-1.3 2006; NAS 2016). The flanges of the CFLDSS specimens were not fastened to the steel loading plates in the test program (Cai and Young 2019a) and in the study of the present paper. This is because, unlike the open sections such as channel sections, the flanges of steel tubular members may not be easy to fasten in practice, e.g., flanges at some location in multiple span of floor joists.

The test specimens and test strengths (P_t) of CFLDSS specimens under the loading conditions of EOF, ETF and EL are shown in Tables 2-4, respectively. The specimens were generally identified by the labelling of three segments. For example, Specimen ETF100×100×3.0N90, the first segment stands for the loading condition of End-Two-Flange (ETF); the second segment means the section dimension of 100×100×3.0 mm; and the third segment indicates that the specimen was loaded with a bearing length (N) of N = 90 mm. The repeated test specimen is indicated by the last letter "r" in the label. The test setups and testing procedures are detailed in Cai and Young (2019a).

FINITE ELEMENT MODELS

General

The finite element models (FEMs) using the ABAQUS program of version 6.20 (2019) were developed to simulate the tests of CFLDSS specimens subjected to concentrated end bearing loads (EOF, ETF and EL). The FEMs were validated by comparing the results from the finite element analysis (FEA) with those test results reported by Cai and Young (2019a), in terms of ultimate strengths, failure modes and load-deformation curves.

Type and size of elements

The shell element type S4R that is a four-node doubly curved element with reduced integration and hourglass control was selected to simulate the CFLDSS tubular specimens. The element S4R was adopted in the FEMs (Li and Young 2017; Li and Young 2018) to successfully simulate the web crippling behaviour of stainless steel tubular members. The solid element type C3D8R was selected to simulate the steel bearing plates. The bearing plates were defined as rigid body as the steel bearing plates in the test program (Cai and Young 2019a) were fabricated by high strength steel which had much higher yield strength than those of the CFLDSS specimens. The mesh sizes in the flat portions of the cross-sections were ranged from 2×2 mm to 10×10 mm (length by width) depending on the dimension of the cross-sections. Similar mesh sizes were adopted on the basis of the sensitivity study by Li and Young (2017; 2018) for the FEMs of ferritic stainless steel tubular members subjected to the same loading conditions as those in this study. Generally, a finer mesh size of five elements at the round corners was employed in order to consider the influence of the corner radius more accurately.

Material properties

The measured engineering stress-strain curves obtained from the coupon tests (Cai and Young 2019a) were converted to true plastic stress-strain curves. The true plastic stress-strain curve was mimicked by means of a piecewise linear stress-strain model, in particular, over the strain-hardening region. Hence, the material non-linearity was incorporated into the FEMs. It should be noted that due to cold working, corner regions of the CFLDSS tubular sections are strengthened, having higher yield strength and ultimate strength than those at the flat regions. Hence, the material properties at the corner regions were also used. The corner material properties were measured by the longitudinal corner coupon tests (Xing and Young 2017; Wang et al. 2019). The corner coupons (Xing and Young 2017; Wang et al.

2019) were extracted from the same batch of CFLDSS members as those investigated by Cai and Young (2019a).

The corner material properties (Xing and Young 2017; Wang et al. 2019) were assigned to the region of curved corners with the extension of twice the section thickness (2*t*) to adjacent flat regions (Li and Young 2018). The tensile flat material properties (Table 1) (Cai and Young 2019a) that obtained in the longitudinal direction of the sections were assigned to the flanges of the sections. In this study, two different cases of material properties were considered at the flat web portions (*h*-2*t*) of the sections. In the first case, the same tensile material properties (Cai and Young 2019a) as those for the flanges were used; while in the second case, the transverse compressive material properties (Table 1) (Cai and Young 2019a) that obtained in the transverse direction of the webs were used. Hence, the effects of tensile and compressive material properties that assigned to the webs of the sections were investigated.

Boundary conditions

The boundary conditions were modelled in accordance with the tests. The geometries, boundary conditions and experimental failure modes of the test specimens were generally symmetric along the middle of the flanges in longitudinal direction for all the three loading conditions (EOF, ETF and EL). Hence, only half of the cross sections (half flanges in longitudinal direction) were considered in the FEMs (e.g., for EOF loading condition in Figure 2(a)). Appropriate boundary conditions were assigned to consider the symmetry of the specimen and the steel bearing plates (solid rigid plates).

The applied loads and reactions were transferred between the steel bearing plates and the specimens. The interfaces between the CFLDSS sections and the steel bearing plates were modelled using the contact pairs. In each contact pair, one surface is defined as master surface while the other as slave surface. The master surfaces were set in the steel bearing plates, whereas the slave surfaces were set in the CFLDSS specimens. The surface-to-surface discretization contact method was employed. The

rounded corners of the section that initially un-contacted to the steel bearing plates may gradually become contacted due to the large deformations as applied load increased. Hence, the section corners adjacent to the flanges were also defined in the slave surfaces (see Figure 2(a)). It should be noted that the contact surfaces were not allowed to penetrate each other. The surface-to-surface contact with a finite sliding option was used. The "hard contact" was used in the normal direction, whereas in the tangential direction, a coefficient of 0.4 was used to consider the friction penalty contact (Li and Young 2017; Li and Young 2018). It should be noted that for the loading condition of EOF, steel stiffening plates were used to prevent web failure of the specimen at mid-span in the tests (Cai and Young 2019a). Similar to the test setup, in the FEM, the out-of-plane deformation of the flat webs at mid-span was restrained (U_x = 0, where U_x means translation in X direction) by a length equal to the width of the steel bearing plate (Figure 2(b)**)**. Proper boundary conditions were assigned to the reference points of the steel bearing plates to simulate the roller support and half round support in the test setup. For example, the boundary conditions of U_x = 0, U_z = 0, R_y = 0 and R_z = 0 (R_y and R_z mean the rotation about direction in Y and Z axes, respectively) were assigned to RP-1 (Figure 2(b)) of the bearing plate to simulate the half round support.

The geometrical nonlinearity of the model is considered by the NLGEOM commend in ABAQUS [35]. The load was applied by specifying axial displacement to the reference point of the steel bearing plate. This was identical to the test program where the load was applied by displacement control (Cai and Young 2019a). The comparison of the tests and FEMs for CFLDSS specimens subjected to different concentrated end bearing loads are illustrated in Figures 3-6, where Figures 3-4 for Specimen EOF120×60×3.0N60, Figures 5-6 for Specimen ETF100×100×3.0N90 and Specimen EL80×150×3.0N90, respectively.

VALIDATION OF FINITE ELEMENT MODELS

The test strengths (P_t) (web crippling strengths) per web obtained from the test program were compared with the numerical strengths (P_{FEA}) per web that were predicted by the FEA, as shown in Tables 2-4. It should be noted that the three specimens that failed near the mid-span instead of web crippling at the ends of the specimens under EOF loading condition (Cai and Young 2019a) were not used in the comparison in Tables 2. As mentioned previously, two cases of material properties were used in the flat web portions of the sections in the FEMs, namely, the first case using the longitudinal tensile material properties and the second case using the transverse compressive material properties. The FEA predictions obtained from the first and second cases were indicated by $P_{FEA\text{-}1}$ and $P_{FEA\text{-}2}$, respectively.

For the loading conditions of EOF, ETF and EL, the respective mean values of the $P_t/P_{FEA\text{-}1}$ are 1.02, 0.99 and 0.97 with the corresponding coefficients of variation (COVs) of 0.096, 0.062 and 0.066 for the first case; while for the second case, the mean values of the $P_t/P_{FEA\text{-}2}$ are 1.00, 0.96 and 0.94 with the corresponding COVs of 0.098, 0.059 and 0.050, as shown in Tables 2-4. Table 5 summarizes the overall comparisons between the tests and FEA for the three loading conditions. It is shown that the mean values of the $P_t/P_{FEA\text{-}1}$ and $P_t/P_{FEA\text{-}2}$ are 0.99 and 0.96 with the corresponding COVs of 0.074 and 0.069. Overall, the two cases of using different material properties in the flat webs are capable to predict the test strengths. However, the first case provides slightly better predictions with the mean value of 0.99 and comparable value of COV than the second case, where the corner material properties (Xing and Young 2017; Wang et al. 2019) in the corners of the sections, longitudinal tensile material properties (Cai and Young 2019a) in the flat portion of webs and flanges of the sections were used. The failure modes and load-web deformation curves obtained from the FE analyses were also compared with those obtained from the test results (Cai and Young 2019a). The comparison of failure mode for Specimen EOF120×60×3.0N60, Specimen ETF100×100×3.0N90 and Specimen EL80×150×3.0N90 are shown in Figures 4-6, respectively. Figure 7 illustrates the comparison of the load-web deformation curves obtained from the tests and FEA, including specimens of

EOF120×60×3.0N30, ETF150×80×3.0N90 and EL100×100×3.0N30, where the test curves were plotted in solid lines while the FEA curves were plotted in solid lines with symbols. The vertical axis plots the ultimate strength per web of the specimens, while the horizontal axis shows the vertical deformation of the webs.

PARAMETRIC STUDY

It is shown from the predictions obtained from the FEA, that using the material properties obtained from longitudinal tensile flat coupons (Cai and Young 2019a) and longitudinal tensile corner coupons (Xing and Young 2017; Wang et al. 2019), are capable to replicate the structural behaviour of CFLDSS tubular sections subjected to concentrated end bearing loads (EOF, ETF and EL), in terms of ultimate strengths (web crippling strengths), failure modes and load-web deformation curves. Hence, after the validation of the FEMs, a parametric study was performed using the validated FEMs to generate numerical data for the CFLDSS tubular sections under the concentrated end bearing loads. The key parameters in the web crippling design of CFLDSS sections include the web slenderness ratio (h/t), bearing length to thickness ratio (N/t) and bearing length to web flat portion ratio (N/h). Same as the test program, the three loading conditions, i.e., EOF, ETF and EL, were considered in the parametric study.

The design of sections and applied bearing lengths in the parametric study are shown in Table 6. In total 12 square and 12 rectangular hollow sections ($H\times B\times t$) were designed. The section dimensions ranged from 60×60×1.5 to 400×200×8 mm. The section inner radius for each specimen was designed based on handbook of the supplier. The radio of r_i/t either equal to 1.0 or 1.5 was used, as shown in Table 6. Hence, the variation of r_i was achieved by different values of t. Each section was loaded with two different bearing lengths (N), i.e., either $N = 0.5B$ or $N = 1.0B$ in each loading condition (EOF,

ETF or EL). Hence, the varied parameters of h/t, N/t and N/h were obtained, and they were ranged from 11.0 to 145.0, 7.5 to 150.0 and 0.26 to 1.36, respectively, as shown in Table 6. The design of specimen length is identical to those adopted in the test program (Cai and Young 2019a). The distance of 1.5H was designed (Cai and Young 2019a) for the clear distance of the two adjacent bearing plate edges in EOF loading condition, and for the clear distance of the specimen free end to the adjacent bearing plate edge in ETF and EL conditions.

The material properties of section 100×100×3.0 (Cai and Young 2019a; Wang et al. 2019) obtained from the coupon tests were used in the parametric analysis in this study. Based on the validations of the FEMs, the longitudinal tensile flat material properties (Cai and Young 2019a) were used for the webs and flanges, while the longitudinal tensile corner material properties (Wang et al. 2019) were used for the corners of the sections. Note that the corner material properties (Wang et al. 2019) were applied to the curved corners and extended to the adjacent flat regions by a distance of 2t. In total, 144 parametric results were generated for the CFLDSS tubular sections subjected to concentrated end bearing loads (EOF, ETF and EL). All these 144 CFLDSS specimens showed pronounce peak loads in the FEA, and generally failed by web crippling except for four specimens that failed near the mid-span but not at the ends of the specimens. These are specimens of EOF60×60×2.0N60, EOF60×60×3.0N60, EOF60×60×4.0N60 and EOF120×120×5.0N120 (Table 7). It should be noted that these four specimens were not included in the comparison of design predicted strengths. The label system for the specimens in the parametric study is identical to that used for the test program as described in the Section of "Summary of experimental investigation" of this paper. The numerical strengths (P_{FEA}) of the specimens per web are shown in Tables 7-9 for the loading conditions of EOF, ETF and EL, respectively.

RELIABILITY ANALYSIS

The web crippling design provisions in this study were assessed by reliability analysis. The analysis was performed by following the Commentary in the ASCE Specification (2002). The design provisions were considered as reliable and probabilistically safe if the value of the reliability index (β) was greater than or equal to the target value of 2.5 in this study. In the calculation of β, the load combination of 1.2DL + 1.6LL was used for the design provisions of ASCE (2002), NAS (2016), Zhou and Young (2008) and the modified DSM (Li and Young 2017; Li and Young 2018), while the combination of 1.35DL + 1.5LL specified in European code (EC0 2005) was used for European design rules (EC3-1.4 2015). The DL and LL represent the dead load and live load, respectively. The DL/LL was set as 0.2 in ASCE (2002). The suggested mean value and COV of the material factor are M_m = 1.10 and F_m = 1.00, respectively; and those of fabrication factor are V_M = 0.10 and V_F = 0.05 in Section 6.2 of ASCE (2002). In addition, a correction factor (C_P) was used to consider the influence of limited test and numerical results. Based on these, the reliability of the design rules were analysed and discussed in the later sections of this paper.

CURRENT DESIGN RULES AND ASSESSMENTS

General

The current design rules found in most specifications for web crippling of cold-formed steel structures are semi-empirical in nature as the theoretical analysis is quite complex. As mentioned in the "Introduction" of this paper, the web crippling design rules in the current international stainless steel specifications (ASCE 2002; AS/NZS 2001; EC3-1.4 2015) are mainly adopted from those of carbon steel design specifications. In addition, these design rules may not adequately account for sections

315 outside the range of variables in the tests and FEA in this study. Nonetheless, the design rules (ASCE
316 2002; AS/NZS 2001; EC3-1.4 2015) were used to calculate the nominal web crippling strengths
317 (unfactored design strengths) per web of the CFLDSS tubular sections subjected to concentrated end
318 bearing loads (EOF, ETF and EL).

319 It should be noted that the design rules specified in the ASCE Specification (2002) and the AS/NZS
320 Standard (2001) are identical, and thus provide identical predictions. Apart from the aforementioned
321 stainless steel design specifications, the unified design equation for different loading conditions (EOF,
322 ETF IOF and ITF) specified in the NAS (2016) was also used in this study. Note that the NAS (2016)
323 is a design specification for cold-formed carbon steel structural members. The design rules found the
324 literature were also adopted in this study, where the unified design equation for web crippling of duplex
325 stainless steel members (Zhou and Young 2008), and the direct strength method (DSM) for web
326 crippling of ferritic stainless steel members (Li and Young 2017; Li and Young 2018) were used. These
327 design rules (Li and Young 2017; Li and Young 2018; Zhou and Young 2008) were assessed for
328 CFLDSS members under the loading conditions of EOF, ETF and EL.

329

330 ## *Design specifications*

331 The differences of the design rules in current stainless steel design specifications (ASCE 2002;
332 AS/NZS 2001 and EC-1.4 2015) are discussed in detail by Cai and Young (2019a). It should be noted
333 that the CFLDSS is not covered in these design specifications, except for EC3-1.4 (2015). The ASCE
334 Specification (2002) and the AS/NZS Standard (2001) provide identical predictions. Hence, the design
335 rules in the ASCE (2002) were adopted, where the web crippling design rules are specified in Section
336 3.3.4 of the ASCE Specification (2002). The web crippling design rules in the EC3-1.4 (2015) may
337 refer to those specified in the EC3-1.3 (2006), where the Section 6.1.7.3 of the EC3-1.3 for "Local
338 transverse forces" was used (EC3-1.3 2006). In addition, the unified design equation (Eq. (1)) specified

in Section G5 of the NAS (2016) for web crippling strengths cold-formed carbon steel structural members was used. This unified web crippling equation for cold-formed carbon steel members was firstly developed by Prabakaran (1993) and Prabakaran and Schuster (1998) for different geometric shapes and four loading cases, including the EOF and ETF in this study. The unified web crippling equation was extended to cover other geometric shapes of carbon steel members, e.g., Behsara and Schuster (2000), and stainless steel tubular members, e.g., Zhou and Young (2008).

$$P = Ct^2 f_{0.2} \sin\theta \left(1 - C_R\sqrt{\frac{r_i}{t}}\right)\left(1 + C_N\sqrt{\frac{N}{t}}\right)\left(1 - C_h\sqrt{\frac{h}{t}}\right) \quad (1)$$

where P = nominal web crippling strength per web, C = overall web crippling coefficient; C_R = inside corner radius coefficient; C_N = bearing length coefficient; C_h = web slenderness coefficient. The coefficients and the application limits specified in NAS (2016) for Eq. (1) are shown in Table 10.

The loading conditions of EOF and ETF are specified in the ASCE (2002) and AS/NZS (2001) specifications. Hence, the corresponding design rules were used to calculate the predicted strengths. It should be noted that the loading condition of EL is not specified in the specifications of ASCE (2002) and NAS (2016). For the purpose of comparison and assessment, the designs of CFLDSS tubular sections for loading conditions of EOF and ETF were both calculated for the EL condition in ASCE (2002) and NAS (2016).

Unified design equation and modified DSM in literature

The aforementioned unified design equation (Eq. (1)) was further developed by Zhou and Young (2008) for web crippling design of cold-formed duplex stainless steel tubular sections subjected to different concentrated bearing loads, including the loading conditions of EOF, ETF and EL. Different sets of coefficients were proposed by Zhou and Young (2008) for different loading conditions. The proposed coefficients and the application limits of Eq. (1) by Zhou and Young (2008) are shown in

Table 10. The modified coefficients for Eq. (1) (Zhou and Young 2008) was also assessed because the grade of CFLDSS is close to that of the cold-formed duplex stainless steel.

The Direct Strength Method (DSM) is an alternative way to determine the strength of cold-formed steel members. The DSM has been developed for the design of cold-formed steel beams and columns, and was documented in the design specifications, for example the NAS (2016). However, the DSM in the current design specifications does not cover the web crippling design of cold-formed steel members. Investigations of DSM for the web crippling design of cold-formed steel open sections were conducted by Keerthan *et al*. (2014) and Natário *et al*. (2016; 2017). Recent studies by Li and Young (2017; 2018) proposed the modified DSM for the web crippling design of cold-formed ferritic stainless steel rectangular and square hollow sections. The proposed design (Li and Young 2017; Li and Young 2018) covers the loading conditions of EOF, ETF and EL, as illustrated in Eq. (2). The nominal web crippling strength per web of a tubular section was determined by Eq. (2). It should be noted that there is no investigation on the DSM for the web crippling design of CFLDSS tubular sections. Hence, the Eq. (2) proposed by Li and Young (2017; 2018) was examined in this study.

$$P_{DSM} = \begin{cases} \gamma P_y & \lambda \le \lambda_k \\ a\left[1 - b\left(\frac{P_{cr}}{P_y}\right)^n\right]\left(\frac{P_{cr}}{P_y}\right)^n P_y & \lambda > \lambda_k \end{cases} \quad (2)$$

where $\lambda = \sqrt{P_y/P_{cr}}$ is the web crippling slenderness ratio. The P_{cr} and P_y are the nominal bearing strengths per web for buckling and yielding, respectively. The calculations of the P_{cr} and P_y for square and rectangular hollow sections refer to the Clause 5.13 of the AS4100 (1998), as adopted by Li and Young (2017; 2018). The corresponding coefficients of a, b, n, γ and λ_k for Eq. (2) are shown in Table 11. The λ_k indicates the cross point of the DSM curve, where the lower bound (conservative manner) of strength predictions are generally adopted for tubular sections with lower web crippling slenderness ratios.

The DSM generally requires aid from computer software to compute the P_{cr}, e.g., the DSM proposed by Natário *et al*. (2016; 2017) for web crippling strength of open sections. However, this is not a necessary for the calculation of P_{cr} in Eq. (2). Instead, the calculations could be done manually by Eqs. (3)-(7) as specified in the AS4100 (1998):

$$P_{cr} = \alpha_c t N_m f_{0.2} \tag{3}$$

where α_c is the slenderness reduction factor as specified in Clause 6.3.3 of the AS4100 (1998), N_m is the mechanism length determined that can be expressed as follows:

$$N_m = N + 2.5R + 0.5h \tag{4}$$

where R is the outer corner radius. Eq. (4) is applicable for the CFLDSS tubular sections subjected to concentrated end bearing loads of EOF, ETF and EL in this study.

$$P_y = \alpha_p t N_m f_{0.2} \tag{5}$$

For interior loading conditions:

$$\alpha_p = \frac{0.5}{k_s}\left[1 + \left(1 - \alpha_{pm}^2\right)\left(1 + \frac{k_s}{k_v} - \left(1 - \alpha_{pm}^2\right)\frac{0.25}{k_v^2}\right)\right] \tag{6}$$

For end loading conditions:

$$\alpha_p = \sqrt{2 + k_s^2} - k_s \tag{7}$$

where $k_s = 2R/t\text{-}1$, $\alpha_{pm} = 1/k_s + 0.5/k_v$ and $k_v = h/t$.

The Clause 5.13 of AS4100 (2018) categorized different loading conditions into end bearing and interior bearing only. It should be noted that the coefficient of α_p for EOF loading condition is determined by Eq. (6) as used by Li and Young (2018). For consistence in the determination of α_p for the three different end loading conditions, the Eq. (7) was used in the calculation of α_p for the EOF, ETF and EL conditions in the modified DSM in present study.

Comparison of test and numerical results with current design predictions

The comparisons of the ultimate strengths (P_u) per web with those predicted by the current design provisions are presented in Tables 7-9 for CFLDSS tubular sections subjected to the loading conditions of EOF, ETF and EL, respectively. The ultimate strengths (P_u) per web represent the strengths either obtained from the tests (P_t) or FEA (P_{FEA}). It should be noted that in the parametric study, the four specimens that did not fail by web crippling were not used in the comparisons, as mentioned previously and shown in Table 7. The predicted strengths for the test specimens were calculated using the measured cross-section dimensions and the corresponding material properties obtained from the tensile coupon tests (see Table 1), whereas the predicted strengths for the FEA specimens were calculated using the nominal cross-section dimensions and the tensile material properties of Section 100×100×3.0 (see Table 1). Note that in the parametric study, the material properties of Section 100×100×3.0 were used for all the specimens.

For the predictions by ASCE (2002), the mean values of the tested and FEA-to-predicted strength ratio (P_u/P_{ASCE}) are 1.33, 1.46, 1.36 (1.90), with the corresponding COVs of 0.141, 0.331 and 0.247 (0.235), for the loading conditions of EOF, ETF and EL, respectively. Note that for the loading condition of EL, the designs for EOF (ETF) were used. The comparisons show that the predictions by EOF design were better than those predicted by ETF design, due to the mean value closer to 1.00 (1.36 compared with 1.90) with the similar values of COV. The predictions by ASCE are overall conservative with the mean values larger than 1.00.

For the predictions by EC3-1.3 (2006), the mean values P_u/P_{EC} are 3.38, 2.62 and 3.41, with the corresponding COVs of 0.218, 0.328 and 0.254, for the loading conditions of EOF, ETF and EL, respectively. Overall, the predictions by EC3-1.3 are very conservative. This is because the web slenderness ratio (h/t) and the actual bearing lengths (N) are not considered in the design provisions of EC3-1.3, however, these key parameters are considered in the design provisions of ASCE (AS/NZS 2001), NAS (2016) and Zhou and Young (2008). Note that the CFLDSS specimen sections had

different web slenderness (h/t) and were loaded by steel plates with different bearing lengths (N) in the range of 30 to 300 mm in this study. However, the EC3-1.3 uses the same bearing length of 10 mm for the design. The conservative predictions provided by EC3-1.3 were also discussed and explained in Cai and Young (2019a).

For the predictions by the unified design equation (Eq. (1)) in NAS (2016), the mean values of the P_u/P_{NAS} are 1.00, 0.82, 1.01 (1.07), with the corresponding COVs of 0.137, 0.224 and 0.208 (0.178), for the loading conditions of EOF, ETF and EL, respectively. Similar to the comparisons for ASCE (2002), the designs for EOF (ETF) were used for the loading condition of EL, where it shows that overall, the mean value obtained from EOF is closer to 1.00 (1.01 compared with 1.07) than that from ETF, however, the predictions are more scattered. While for the predictions by Zhou and Young (2008) using the modified coefficients for Eq. (1) (NAS 2016), the mean values of $P_u/P_{Z\&Y}$ are 0.97, 1.13 and 1.05, with the corresponding COVs of 0.136, 0.240 and 0.217, for the loading conditions of EOF, ETF and EL, respectively.

For the predictions by DSM (Li and Young 2017; Li and Young 2018), the mean values $P_u/P_{L\&Y}$ are 1.05, 1.10 and 1.24, with the corresponding COVs of 0.071, 0.075 and 0.115, for the loading conditions of EOF, ETF and EL, respectively. Overall, the predictions by DSM (Li and Young 2017; Li and Young 2018) are conservative as the mean values are larger than 1.00. It was found that the DSM (Li and Young 2017; Li and Young 2018) provided less scattered predictions than those predictions by ASCE (2002), EC3-1.3 (2006), NAS (2016), and Zhou and Young (2008), as the COV is the smallest in the comparisons for the three loading conditions, as shown in Tables 7-9.

The comparisons of the ultimate strengths (P_u) per web with those predicted by the current design provisions are shown in Figures 8-12. The comparisons were plotted against the web slenderness ratio of h/t for the CFLDSS specimens. Generally, the predictions by ASCE (2002) and EC3-1.3 (2006) are more conservative for the small values of h/t, which is stocky webs. The predictions by Zhou and Young (2008) are generally conservative for the lower values of h/t ($h/t < 45$), however, the predictions

become unconservative for the higher values of h/t (h/t > 75). The predictions provided by Li and Young (2017; 2018) are generally conservative, in particular for the loading condition of EL (see Figure 12). It should be noted that the predictions by ASCE (2002) and NAS (2016) for EL condition, the superscripts of "$^{\#}$" and "*" indicate that the predictions were calculated by the design rules for loading conditions of EOF and ETF, respectively (see Figures 8 and 10). For the EL condition predicted by ASCE (2002) and NAS (2016), it was found that using the design rules of EOF provided less conservative predictions than using the design rules of ETF. Overall, the predictions tended to be more conservative for very low slenderness of the web in the sections (see Figures 8-12), such as specimens ETF20×50×1.5N30 and EL20×50×1.5N50 of test specimens, and specimens ETF60×60×4.0N60 and EL60×60×4.0N60 of parametric studies. For these specimens, the failure of web crippling occurred at the later loading stage, hence, ultimate loads of these sections were more benefited from the strain hardening of the material.

The reliability of the aforementioned design provisions for the CFLDSS tubular sections under concentrated end bearing loads was assessed by the reliability analysis. The respective resistance factors (ϕ) for the design rules as recommended by the ASCE (2002), EC3-1.4 (2015), NAS (2016), Zhou and Young (2008) and Li and Young (2017; 2018) are shown in Tables 7-9. These values were used in the calculations of reliability index (β). It was found that all the current design provisions for the EOF loading condition are probabilistically safe and reliable, as the values of β are larger than the target value of 2.50 (see Table 7). The current design provisions for the ETF loading condition are also probabilistically safe and reliable, except for NAS (2016) due to the β = 1.27 which is smaller than 2.50. It is shown that the coefficients specified in the NAS (2016) and those proposed by Zhou and Young (2008) for the unified design equation (Eq. (1)) are not reliable for the loading condition of EL, due to the values of β are smaller than 2.50, as shown in Table 9.

PROPOSED DESIGN RULES AND ASSESSMENTS

General

As discussed in the previous section of this paper, the predictions by the ASCE (2002), EC3-1.3 (2006) and the modified DSM (Eq. (2)) (Li and Young 2017; Li and Young 2018) are generally conservative and reliable, in particular, very conservative predictions by EC3-1.3 (2006). The predictions by the unified design equation (Eq. (1)) in NAS (2016) are not reliable for the loading conditions of ETF and EL. The predictions by Zhou and Young (2008) are not reliable for the EL condition. Hence, efforts were made for the improvements of the design of CFLDSS tubular sections under concentrated end bearing loads in this study, where new coefficients are proposed for the unified design equation (Eq. (1)) in NAS (2016) and the modified DSM (Li and Young 2017; Li and Young 2018).

Unified design equation with modified coefficients

Three new sets of coefficients are proposed for the unified design equation (Eq. (1)) in the NAS (2016). The three sets of coefficients are proposed for CFLDSS tubular sections under the loading conditions of EOF, ETF and EL. The coefficients were calibrated against the 47 test results (Cai and Young 2019a) and 140 numerical results obtained in this study. Note that the four numerical results of EOF loading condition (see Table 7) were not included in the calibration as those specimens did not fail by web crippling. The new coefficients of C, C_R, C_N, and C_h for the unified design equation Eq. (1) (NAS 2016) are reported in Table 10. The overall web crippling coefficient, C = 5.0, C = 3.5 and C = 4.8 are proposed for the loading conditions of EOF, ETF and EL, respectively. It should be noted that different values of coefficients (C_R, C_N, and C_h) are specified in NAS (2016) and Zhou and Young (2008) for the three loading conditions of EOF, ETF and EL. However, constant coefficients of C_R = 0.40, C_N = 0.55 and C_h = 0.032 are proposed in this study (see Table 10) regardless of different loading conditions (EOF, ETF and EL). In addition, a relatively larger value of resistance factor of ϕ = 0.85 is proposed

compared with ϕ = 0.80 in NAS (2016) and ϕ = 0.70 in Zhou and Young (2008) for the EOF loading condition. These proposed coefficients for Eq. (1) are applicable for CFLDSS square and rectangular hollow sections having stiffened or partially stiffened flanges with the limits for h/t, r_i/t, N/t, and N/h, as shown in Table 10.

Modified direct strength method

It has been shown that the modified DSM design equation (Eq. (2)) proposed by Li and Young (2017; 2018) for the web crippling strength of cold-formed ferritic stainless steel tubular sections generally provided conservative predictions for the web crippling strength of CFLDSS tubular sections in this study, in particular for the EL condition. Hence, improvements on the modified DSM design equation (Eq. (2)) were made by proposing three new sets of coefficients. The coefficients were also calibrated against the 47 test results (Cai and Young 2019a) and 140 numerical results as those for the Eq. (1). The new coefficients of a, b, n, λ_k, and γ for Eq. (2) are reported in Table 11. Similar to those suggested by Li and Young (2017; 2018), different values of a, λ_k and γ are proposed for different loading conditions. However, the constant coefficients of b = 0.20 and n = 0.50 are proposed regardless of different loading conditions. These proposed coefficients (see Table 11**)** for Eq. (2) are applicable for CFLDSS square and rectangular hollow sections having stiffened or partially stiffened flanges with the limits for $10 \leq h/t \leq 145$, $r_i/t \leq 2.0$, $N/t \leq 150$ and $N/h \leq 1.5$.

Comparison of test and numerical results with proposed design predictions

The comparisons of the test and numerical results with those predicted by the design equations (Eq. (1) and Eq. (2)) using the newly proposed coefficients are also presented in Tables 7-9, for the loading conditions of EOF, ETF and EL, respectively. The predictions by Eq. (1) and Eq. (2) using the new

527 coefficients were represented by P_1 and P_2, respectively. In the calculations, the material properties
528 were used in the same criteria as those described in the previous section of this paper.

529 For the predictions by the unified design equation (Eq. (1)) using the new coefficients in Table 10, the
530 mean values of the P_u/P_1 are 1.00, 1.07 and 1.02, with the corresponding COVs of 0.115, 0.204 and
531 0.144, for the loading conditions of EOF, ETF and EL, respectively. The predictions by Eq. (1) using
532 the newly proposed coefficients are probabilistically safe and reliable as all the reliability indexes (β)
533 are larger than the target value of 2.50. Figure 13 illustrates the comparison of the ultimate strengths
534 (P_u) per web with those predicted by the proposed unified design equation (P_1) for the CFLDSS tubular
535 sections subjected to the loading conditions of EOF, ETF and EL.

536 While for the predictions by the modified DSM using the new coefficients in Table 11, the mean values
537 of the P_u/P_2 are 1.02, 1.01 and 1.00, with the corresponding COVs of 0.070, 0.078 and 0.112, for the
538 loading conditions of EOF, ETF and EL, respectively. The predictions by Eq. (2) with the proposed
539 new coefficients are all probabilistically safe and reliable ($\beta > 2.5$). Figure 14 illustrates the comparison
540 of the ultimate strengths (P_u) per web with those predicted by the modified DSM (P_2) using the new
541 coefficients for CFLDSS tubular sections subjected to the loading conditions of EOF, ETF and EL.
542 Similar to those shown in Figures 8-12, the predictions (see Figures 13-14) are generally more
543 conservative for the very low web slenderness of the sections. This is due to the effect of stain
544 hardening of the material, as discussed previously. In addition, Figures 15-17 show the comparisons
545 of the test and numerical results with the DSM curves for the loading conditions of EOF, ETF and EL,
546 respectively. In each figure, the ratio of P_u/P_y were plotted against the web crippling slenderness ratio
547 of $(P_y/P_{cr})^{0.5}$. Generally, it is shown that the proposed DSM curves in this study provide better fitting
548 than the DSM curves proposed by Li and Young (2017; 2018).

549

550

CONCLUSIONS

Non-linear finite element models (FEMs) were developed for the web crippling of cold-formed lean duplex stainless steel (CFLDSS) tubular sections subjected to concentrated end bearing loads, namely, the loading conditions of End-One-Flange (EOF), End-Two-Flange (ETF) and end loading (EL). The FEMs were verified against the test results in terms of ultimate strengths, failure modes and load-deformation curves. An extensive parametric study of 144 CFLDSS tubular sections under the three loading conditions was performed by using the verified FEMs. The specimens in parametric study were designed such that the key parameters were examined. The key parameters include the ratios of flat web height to thickness, bearing length to web thickness and bearing length to flat web height.

The web crippling strengths obtained from the finite element analysis and the tests were compared with the nominal strengths calculated using the current design rules in the international specifications (ASCE 2002, AS/NZS 2001, and EC3-1.4 2015; EC3-1.3 2006; NAS 2016), and those in the literature (the unified design equation (Zhou and Young 2008) and modified direct strength method (DSM) (Li and Young 2017; Li and Young 2018)). The reliability of the design provisions was assessed by reliability analysis. It was found that the predictions by the ASCE 2002, EC3 (2006; 2015) and the modified DSM (Eq. (2)) (Li and Young 2017; Li and Young 2018) are overall conservative and reliable. The predictions by the NAS (2016) are not reliable for the loading conditions of ETF and EL. The predictions by the unified design equation (Zhou and Young 2008) are not reliable for the EL condition.

New sets of coefficients are proposed for the unified design equation in NAS (2016) and the modified DSM for web crippling design of CFLDSS square and rectangular hollow sections subjected to concentrated end bearing loads of EOF, ETF and EL. The proposed coefficients were calibrated against the test results and numerical results. By using the newly proposed coefficients in the design calculations, it is shown that the predictions by the unified design equation in NAS (2016) and the modified DSM are more accurate than those aforementioned predictions, and probabilistically safe and

reliable. Therefore, the newly proposed coefficients for the unified design equation in NAS (2016) and the modified DSM are applicable for web crippling (loading conditions of EOF, ETF and EL) design of CFLDSS square and rectangular hollow sections with limits of $10 \leq h/t \leq 145$, $r_i/t \leq 2.0$, $N/t \leq 150$ and $N/h \leq 1.5$. The flanges of the CFLDSS tubular sections are stiffened or partially stiffened that unfastened to the supports.

DATA AVAILABILITY STATEMENT

Data Availability Statement All data, models, and code generated or used during the study appear in the published article.

REFERENCES

ABAQUS. (2019). "Analysis User's Manual", ABAQUS, Inc., Version 6.20, 2019.

Australian Standard (AS). (1998). "Steel structures." AS 4100, Sydney, Australia: Standards Australia; 1998.

ASCE. (2002). "Specification for the design of cold-formed stainless steel structural members." American Society of Civil Engineers (ASCE), ASCE Standard, SEI/ASCE-8-02, Reston, Virginia, 2002.

AS/NZS. (2001). "Cold-formed stainless steel structures." AS/NZS 4673:2001, Australian/New Zealand Standard (AS/NZS), Standards Australia, Sydney, Australia, 2001.

Beshara, B., and Schuster, P.M. (2000). "Web crippling data and calibrations of cold formed steel members." *Final Report*, University of Waterloo, Waterloo, Canada.

Bock, M., Arrayago, I., Real, E. and Mirambell, E. (2013). "Study of web crippling in ferritic stainless steel cold formed sections." *Thin-Walled Structures*, 69: 29-44.

599 Cai, Y. and Young, B. (2014a). “Structural behavior of cold-formed stainless steel bolted connections.”
600 *Thin-Walled Structures,* 83: 147-156.

601 Cai, Y. and Young, B. (2014b). “Behavior of cold-formed stainless steel single shear bolted
602 connections at elevated temperatures.” *Thin-Walled Structures,* 75: 63-75.

603 Cai, Y. and Young, B. (2014c). “Transient state tests of cold-formed stainless steel single shear bolted
604 connections.” *Engineering Structures,* 81: 1-9.

605 Cai, Y. and Young, B. (2015). “High temperature tests of cold-formed stainless steel double shear
606 bolted connections.” *Journal of Constructional Steel Research,* 104: 49-63.

607 Cai, Y. and Young, B. (2019a). “Web crippling of lean duplex stainless steel tubular sections under
608 concentrated end bearing loads.” *Thin-Walled Structure*s, 134: 29-39.

609 Cai, Y. and Young, B. (2019b). “Cold-formed lean duplex stainless steel tubular members under
610 concentrated interior bearing loads.” *Journal of Structural Engineering*, ASCE. 145(7): 04019056.

611 dos Santos, G.B., Gardner L. and Kucukler M. (2018). “Experimental and numerical study of stainless
612 steel I-sections under concentrated internal one-flange and internal two-flange loading.”
613 *Engineering Structures,* 175: 355-370.

614 dos Santos, G.B. and Gardner L. (2019). “Testing and numerical analysis of stainless steel I-sections
615 under concentrated end-one-flange loading.” *Journal of Constructional Steel Research*, 157: 271-
616 281.

617 EC0. (2005). “Eurocode 0: basis of structural design.” EN 1990:2002+A1:2005. Brussels, Belgium:
618 European committee for standardization; 2005.

619 EC3-1.3. (2006). “Eurocode 3: Design of steel structures - Part 1–3: General rules – Supplementary
620 rules for cold-formed members and sheeting.” EN 1993-1-3, Brussels, Belgium: European
621 committee for standardization; 2006.

EC3-1.4. (2015). “Eurocode 3. Design of steel structures - Part 1.4: General rules - Supplementary rules for stainless steels.” EN 1993-1-4:2006+A1:2015, Brussels, Belgium, European Committee for Standardization, 2015.

Gardner, L. and Baddoo, N.R. (2006). “Fire testing and design of stainless steel structures.” *Journal of Constructional Steel Research,* 62(6): 532–543.

Gardner, L., Talja, A. and Baddoo, N.R. (2006). “Structural design of high-strength austenitic stainless steel.” *Thin-Walled Structures*, 44: 517-528.

Huang, Y. and Young, B. (2012). “Material properties of cold-formed lean duplex stainless steel sections.” *Thin-Walled Structures*, 54: 72-81.

Huang, Y. and Young, B. (2013). “Tests of pin-ended cold-formed lean duplex stainless steel columns.” *Journal of Constructional Steel Research*, 82: 203-215.

Huang, Y. and Young, B. (2014). “Experimental and numerical investigation of cold-formed lean duplex stainless steel flexural members.” *Thin-Walled Structures,* 73: 216-228.

Keerthan P, Mahendran M, Steau E. (2014). “Experimental study of web crippling behaviour of hollow flange channel beams under two flange load cases.” *Thin-Walled Structure*; 85:207-19.

Li, H-T. and Young, B. (2017). “Cold-formed ferritic stainless steel tubular structural members subjected to concentrated bearing loads.” *Engineering Structures*, 145: 392-405.

Li, H-T. and Young, B. (2018). “Web crippling of cold-formed ferritic stainless steel square and rectangular hollow sections.” *Engineering Structures*, 176: 968-980.

Natário P, Silvestre N, Camotim D. (2017). “Web crippling of beams under ITF loading: a novel DSM-based design approach.” *Journal of Constructional Steel Research*; 128:812-24.

Natário P, Silvestre N, Camotim D. (2016). “Direct strength prediction of web crippling failure of beams under ETF loading.” *Thin-Walled Structures*; 98, Part B:360-74.

North American Specification (NAS) (2016). "North American Specification for the design of cold-formed steel structural members." AISI S100–16, Washington D. C., USA: American Iron and Steel Institute (AISI); 2016.

Prabakaran, K. (1993). Web Crippling of Cold Formed Steel Sections, *Project Report*, Department of Civil Engineering, University of Waterloo, Waterloo, Ontario, Canada, April.

Prabakaran, K., and Schuster, P.M. (1998). "Web crippling of cold-formed steel members." *Proceedings of the 14th International Specialty Conference on Cold formed Steel Structures*, St. Louis, University of Missouri-Rolla, Mo., 151-164.

Saliba, N. and Gardner, L. (2013a). "Cross-section stability of lean duplex stainless steel welded I-sections." *Journal of Constructional Steel Research*, 18: 1-14.

Saliba, N. and Gardner L. (2013b). "Experimental study of the shear response of lean duplex stainless steel plate girders." *Engineering Structures*, 46: 375-391.

Saliba N., Real, E., Gardner, L. (2014). "Shear design recommendations for stainless steel plate girders." *Engineering Structures*, 59: 220-228.

Theofanous, M. and Gardner L. (2009). "Testing and numerical modelling of lean duplex stainless steel hollow section columns." *Engineering Structures*, 31: 3047-3058.

Theofanous, M. and Gardner L. (2010). "Experimental and numerical studies of lean duplex stainless steel beams." *Journal of Constructional Steel Research*, 66: 816-825.

Wang, F., Young, B. and Gardner, L. (2019). "Experimental Study of Square and Rectangular CFDST Sections with Stainless Steel Outer Tubes under Axial Compression." *Journal of Structural Engineering*, ASCE, 145(11): 04019139.

Xing, B. and Young, B. (2017). "Experimental investigation of concrete-filled lean duplex stainless steel RHS stub columns." Proceedings of 16th International Symposium on Tubular Structures (ISTS16) 2017, Eds. Heidarpour A. and ZHAO X.-L. Melbourne, Australia. 95-100.

669 Young, B. Hancock, G. J. (2001). “Design of cold-formed channels subjected to web crippling.”
670 *Journal of Structural Engineering*, 127(10): 1137-1034.

671 Zhao, O., Rossi, B., Gardner, L. and Young, B. (2015a). “Behaviour of structural stainless steel cross-
672 sections under combined loading – Part I: Experimental study.” *Engineering Structures*, 89, 236-
673 246.

674 Zhao, O., Rossi, B., Gardner, L. and Young, B. (2015b). “Behaviour of structural stainless steel cross-
675 sections under combined loading – Part II: Numerical modelling and design.” *Engineering*
676 *Structures*, 89, 247-259.

677 Zhao, O., Afshan, S. and Gardner, L. (2017). “Structural response and continuous strength method
678 design of slender stainless steel cross-sections.” *Engineering Structures*, 140, 14-25.

679 Zhao, O. and Gardner, L. (2018). “The continuous strength method for the design of mono-symmetric
680 and asymmetric stainless steel cross-sections in bending.” *Journal of Constructional Steel Research*,
681 150, 141-152.

682 Zhou, F. and Young, B. (2006). “Cold-formed stainless steel sections subjected to web crippling.”
683 *Journal of Structural Engineering*, 132(1): 134-144.

684 Zhou, F. and Young, B. (2007a). “Experimental and numerical investigations of cold-formed stainless
685 steel tubular sections subjected to concentrated bearing load.” *Journal of Constructional Steel*
686 *Research*, 63(11): 1452-1466.

687 Zhou, F. and Young, B. (2007b). “Cold-formed high-strength stainless steel tubular sections subjected
688 to web crippling.” *Journal of Structural Engineering*, 133(3): 368-377.

689 Zhou, F. and Young, B. (2008). “Web crippling of cold-formed stainless steel tubular sections.”
690 *Advances in Structural engineering*, 11(6): 679-691.

691
692
693
694
695

Table 1: Material properties of lean duplex stainless steel (Cai and Young 2019a)

Stainless steel grade	Section $H\times B\times t$ (mm)	E_T	E_C	$f_{0.2,T}$	$f_{0.2,C}$	$\varepsilon_{f,T}$
		GPa	GPa	MPa	MPa	%
EN 1.4162	50×20×1.5	194	212	656	611	42.2
EN 1.4062	60×40×2.0	199	211	600	627	40.3
	60×120×3.0	206	215	620	727	38.5
	80×150×3.0	194	214	491	546	43.3
	100×100×3.0	202	209	557	551	43.1
	120×60×3.0	206	215	620	611	38.5
	150×80×3.0	194	208	491	518	43.3

Table 2: Comparison of test strengths with FE strengths for EOF loading condition

Specimen	P_t (kN)	$P_{FEA\text{-}1}$ (kN)	$P_{FEA\text{-}2}$ (kN)	$P_t/P_{FEA\text{-}1}$	$P_t/P_{FEA\text{-}2}$
EOF60×120×3.0N60	48.9*	53.4	54.7	0.92	0.89
EOF80×150×3.0N60	35.7*	35.2	36.3	1.02	0.98
EOF80×150×3.0N90	42.7*	44.2	45.5	0.97	0.94
EOF100×100×3.0N30	39.6*	32.1	32.6	1.24	1.21
EOF120×60×3.0N30	34.3*	33.6	33.7	1.02	1.02
EOF120×60×3.0N60	46.7*	48.8	49.1	0.96	0.95
EOF150×80×3.0N30	23.6*	22.9	23.0	1.03	1.03
EOF150×80×3.0N90	37.3*	38.2	39.5	0.98	0.95
			Mean	1.02	1.00
			COV	0.096	0.098

Note: "*" means data presented in Cai and Young (2019a).

Table 3: Comparison of test strengths with FE strengths for ETF loading condition

Specimen	P_t (kN)	P_{FEA-1} (kN)	P_{FEA-2} (kN)	P_t/P_{FEA-1}	P_t/P_{FEA-2}
ETF60×40×2.0N30	13.2*	13.9	14.3	0.95	0.92
ETF60×40×2.0N30-r	13.9*	13.9	14.2	1.00	0.98
ETF60×120×3.0N60	44.5*	43.3	47.3	1.03	0.94
ETF60×120×3.0N90	56.7*	55.8	61.0	1.02	0.93
ETF80×150×3.0N60	24.1*	24.5	25.8	0.98	0.93
ETF80×150×3.0N150	44.3*	43.1	45.0	1.03	0.98
ETF100×100×3.0N30	25.1*	25.5	25.6	0.98	0.98
ETF100×100×3.0N90	42.4*	39.9	40.4	1.06	1.05
ETF100×100×3.0N90-r	43.5*	40.9	41.4	1.06	1.05
ETF120×60×3.0N30	24.5*	27.5	27.6	0.89	0.89
ETF120×60×3.0N60	29.9*	35.3	35.3	0.85	0.85
ETF150×80×3.0N30	19.2*	19.3	19.7	0.99	0.97
ETF150×80×3.0N90	27.2*	27.0	27.8	1.01	0.98
			Mean	0.99	0.96
			COV	0.062	0.059

Note: "*" means data presented in Cai and Young (2019a).

Table 4: Comparison of test strengths with FE strengths for EL condition

Specimen	P_t (kN)	P_{FEA-1} (kN)	P_{FEA-2} (kN)	P_t/P_{FEA-1}	P_t/P_{FEA-2}
EL60×40×2.0N30	17.6*	19.5	19.9	0.90	0.88
EL60×40×2.0N50	22.0*	23.8	24.4	0.92	0.90
EL60×120×3.0N60	51.9*	49.2	53.9	1.05	0.96
EL60×120×3.0N120	74.7*	69.2	74.5	1.08	1.00
EL80×150×3.0N60	33.2*	32.3	34.1	1.03	0.97
EL80×150×3.0N150	49.9*	51.1	53.3	0.98	0.94
EL100×100×3.0N30	33.3*	32.9	33.1	1.01	1.01
EL100×100×3.0N90	48.2*	47.6	48.4	1.01	1.00
EL100×100×3.0N90-r	47.8*	50.1	50.9	0.95	0.94
EL120×60×3.0N30	31.4*	34.2	34.3	0.92	0.92
EL120×60×3.0N60	38.7*	43.1	43.0	0.90	0.90
EL120×60×3.0N60-r	36.6*	43.7	43.7	0.84	0.84
EL150×80×3.0N30	24.8*	25.8	26.7	0.96	0.93
EL150×80×3.0N90	32.5*	34.0	35.1	0.96	0.93
EL150×80×3.0N90-r	33.2*	34.1	35.1	0.97	0.95
			Mean	0.97	0.94
			COV	0.066	0.050

Note: "*" means data presented in Cai and Young (2019a).

Table 5: Summary of FE verification

Loading condition	Number		P_t/P_{FEA-1}	P_t/P_{FEA-2}
EOF, ETF, EL	36	Mean	0.99	0.96
		COV	0.074	0.069

763 **Table 6:** Design of CFLDSS specimens for parametric study

Section ($H\times B\times t$)	N (mm)	r_i/t	h/t	N/t	N/h
60×60×1.5	30	1.00	36.0	20.0	0.56
60×60×1.5	60	1.00	36.0	40.0	1.11
60×60×2.0	30	1.00	26.0	15.0	0.58
60×60×2.0	60	1.00	26.0	30.0	1.15
60×60×3.0	30	1.00	16.0	10.0	0.63
60×60×3.0	60	1.00	16.0	20.0	1.25
60×60×4.0	30	1.00	11.0	7.5	0.68
60×60×4.0	60	1.00	11.0	15.0	1.36
120×120×2.0	60	1.50	55.0	30.0	0.55
120×120×2.0	120	1.50	55.0	60.0	1.09
120×120×2.5	60	1.50	43.0	24.0	0.56
120×120×2.5	120	1.50	43.0	48.0	1.12
120×120×3.5	60	1.50	29.3	17.1	0.59
120×120×3.5	120	1.50	29.3	34.3	1.17
120×120×5.0	60	1.50	19.0	12.0	0.63
120×120×5.0	120	1.50	19.0	24.0	1.26
300×300×2.0	150	1.50	145.0	75.0	0.52
300×300×2.0	300	1.50	145.0	150.0	1.03
300×300×3.5	150	1.50	80.7	42.9	0.53
300×300×3.5	300	1.50	80.7	85.7	1.06
300×300×4.0	150	1.50	70.0	37.5	0.54
300×300×4.0	300	1.50	70.0	75.0	1.07
300×300×6.0	150	1.00	46.0	25.0	0.54
300×300×6.0	300	1.00	46.0	50.0	1.09
100×80×1.5	40	1.00	62.7	26.7	0.43
100×80×1.5	80	1.00	62.7	53.3	0.85
100×80×2.0	40	1.00	46.0	20.0	0.43
100×80×2.0	80	1.00	46.0	40.0	0.87
100×80×2.5	40	1.00	36.0	16.0	0.44
100×80×2.5	80	1.00	36.0	32.0	0.89
100×80×3.0	40	1.00	29.3	13.3	0.45
100×80×3.0	80	1.00	29.3	26.7	0.91
200×150×2.0	75	1.50	95.0	37.5	0.39
200×150×2.0	150	1.50	95.0	75.0	0.79
200×150×2.5	75	1.50	75.0	30.0	0.40
200×150×2.5	150	1.50	75.0	60.0	0.80
200×150×4.0	75	1.50	45.0	18.8	0.42
200×150×4.0	150	1.50	45.0	37.5	0.83
200×150×4.5	75	1.00	40.4	16.7	0.41
200×150×4.5	150	1.00	40.4	33.3	0.82
400×200×3.0	100	1.50	128.3	33.3	0.26
400×200×3.0	200	1.50	128.3	66.7	0.52
400×200×4.0	100	1.50	95.0	25.0	0.26
400×200×4.0	200	1.50	95.0	50.0	0.53
400×200×6.0	100	1.00	62.7	16.7	0.27
400×200×6.0	200	1.00	62.7	33.3	0.53
400×200×8.0	100	1.00	46.0	12.5	0.27
400×200×8.0	200	1.00	46.0	25.0	0.54

764

Table 7: Comparison of test and FE strengths with design predicted strengths for EOF loading condition

Specimen	P_u (P_t or P_{FEA})	P_u/P_{ASCE}	P_u/P_{EC}	P_u/P_{NAS}	$P_u/P_{Z\&Y}$	$P_u/P_{L\&Y}$	P_u/P_1	P_u/P_2
	(kN)							
EOF60×120×3.0N60	48.9	1.46	3.48	1.03	0.92	0.88	0.91	0.85
EOF80×150×3.0N60	35.7	1.28	3.08	1.04	1.25	1.04	1.24	1.09
EOF80×150×3.0N90	42.7	1.41	3.67	1.09	1.29	0.98	1.28	1.03
EOF100×100×3.0N30	39.6	1.32	2.99	1.17	1.11	1.20	1.12	1.17
EOF120×60×3.0N30	34.3	1.17	2.45	0.93	0.88	1.02	0.90	0.99
EOF120×60×3.0N60	46.7	1.45	3.32	1.03	0.92	1.04	0.94	1.00
EOF150×80×3.0N30	23.6	0.96	2.02	0.87	1.08	1.02	1.12	1.00
EOF150×80×3.0N90	37.3	1.26	3.17	0.98	1.13	1.05	1.16	1.03
EOF60×60×1.5N30	10.1	1.31	2.80	1.03	0.94	1.02	0.96	0.98
EOF60×60×1.5N60	15.7	1.74	4.35	1.28	1.14	1.08	1.15	1.04
EOF60×60×2.0N30	16.6	1.24	2.75	1.03	0.94	0.99	0.95	0.95
EOF60×60×2.0N60*	23.2	-	-	-	-	-	-	-
EOF60×60×3.0N30	33.1	1.13	2.62	0.99	0.93	0.98	0.92	0.96
EOF60×60×3.0N60*	36.9	-	-	-	-	-	-	-
EOF60×60×4.0N30	51.4	1.00	2.40	0.92	0.87	0.99	0.86	1.01
EOF60×60×4.0N60*	50.4	-	-	-	-	-	-	-
EOF120×120×2.0N60	17.3	1.31	2.94	0.94	0.96	1.07	1.00	1.04
EOF120×120×2.0N120	24.9	1.53	4.22	1.07	1.05	1.05	1.09	1.01
EOF120×120×2.5N60	26.6	1.32	3.01	0.98	1.00	1.06	1.03	1.03
EOF120×120×2.5N120	39.8	1.65	4.51	1.16	1.16	1.09	1.18	1.06
EOF120×120×3.5N60	47.9	1.25	2.93	0.97	1.01	1.01	1.02	0.99
EOF120×120×3.5N120	73.3	1.67	4.49	1.19	1.20	1.07	1.21	1.04
EOF120×120×5.0N60	85.8	1.12	2.72	0.92	0.97	0.96	0.97	0.95
EOF120×120×5.0N120*	118.7	-	-	-	-	-	-	-
EOF300×300×2.0N150	14.4	0.99	2.44	0.64	0.63	0.89	0.71	0.85
EOF300×300×2.0N300	18.4	0.89	3.13	0.62	0.60	0.77	0.68	0.73
EOF300×300×3.5N150	53.2	1.26	3.26	0.87	0.87	1.07	0.93	1.03
EOF300×300×3.5N300	72.0	1.32	4.41	0.92	0.90	0.98	0.95	0.94
EOF300×300×4.0N150	70.8	1.31	3.39	0.92	0.92	1.09	0.97	1.05
EOF300×300×4.0N300	97.2	1.41	4.66	0.98	0.96	1.02	1.01	0.98
EOF300×300×6.0N150	173.7	1.38	3.82	1.06	0.95	1.08	0.98	1.04
EOF300×300×6.0N300	248.9	1.65	5.48	1.20	1.06	1.05	1.08	1.01
EOF100×80×1.5N40	9.9	1.29	2.75	0.97	0.87	1.07	0.92	1.03
EOF100×80×1.5N80	13.6	1.46	3.78	1.05	0.92	1.04	0.97	0.99
EOF100×80×2.0N40	17.2	1.28	2.84	1.01	0.92	1.06	0.95	1.02
EOF100×80×2.0N80	24.5	1.56	4.05	1.15	1.02	1.06	1.04	1.02
EOF100×80×2.5N40	25.7	1.24	2.84	1.02	0.93	1.03	0.95	0.99

EOF100×80×2.5N80	37.3	1.59	4.12	1.19	1.06	1.06	1.08	1.02
EOF100×80×3.0N40	35.3	1.20	2.79	1.01	0.93	1.00	0.94	0.97
EOF100×80×3.0N80	53.4	1.62	4.23	1.24	1.11	1.08	1.12	1.05
EOF200×150×2.0N75	15.7	1.22	2.66	0.84	0.84	1.10	0.92	1.05
EOF200×150×2.0N150	20.2	1.24	3.43	0.84	0.83	1.00	0.90	0.96
EOF200×150×2.5N75	25.3	1.28	2.86	0.91	0.92	1.13	0.98	1.09
EOF200×150×2.5N150	34.0	1.40	3.86	0.96	0.95	1.08	1.01	1.04
EOF200×150×4.0N75	61.2	1.24	2.93	0.95	0.98	1.08	1.01	1.05
EOF200×150×4.0N150	88.3	1.55	4.23	1.10	1.10	1.12	1.13	1.08
EOF200×150×4.5N75	85.3	1.28	3.20	1.04	0.95	1.07	0.98	1.04
EOF200×150×4.5N150	123.8	1.62	4.65	1.21	1.08	1.11	1.10	1.07
EOF400×200×3.0N100	31.1	1.20	2.53	0.80	0.81	1.13	0.91	1.07
EOF400×200×3.0N200	37.5	1.16	3.05	0.76	0.75	1.03	0.84	0.98
EOF400×200×4.0N100	58.9	1.26	2.82	0.90	0.92	1.20	1.00	1.15
EOF400×200×4.0N200	72.7	1.30	3.48	0.88	0.88	1.12	0.95	1.07
EOF400×200×6.0N100	142.4	1.25	3.13	1.01	0.92	1.15	0.98	1.10
EOF400×200×6.0N200	182.5	1.41	4.02	1.04	0.93	1.12	0.97	1.07
EOF400×200×8.0N100	237.1	1.18	3.04	1.00	0.93	1.08	0.96	1.04
EOF400×200×8.0N200	326.5	1.46	4.19	1.12	1.01	1.14	1.04	1.10
Mean		1.33	3.38	1.00	0.97	1.05	1.00	1.02
COV		0.141	0.218	0.137	0.136	0.071	0.115	0.070
Resistance factor, ϕ		0.70	0.91	0.80	0.70	0.85	0.85	0.85
Reliability index, β		4.14	5.46	2.65	3.03	2.91	2.55	2.79

*Note: Specimen failed near mid-span, which were not included in the comparison.

Table 8: Comparison of test and FE strengths with design predicted strengths for ETF loading condition

Specimen	P_u (P_t or P_{FEA})	P_u/P_{ASCE}	P_u/P_{EC}	P_u/P_{NAS}	$P_u/P_{Z\&Y}$	$P_u/P_{L\&Y}$	P_u/P_1	P_u/P_2
	(kN)							
ETF20×50×1.5N30	18.0	3.05	4.59	1.16	1.84	1.44	1.60	1.44
ETF20×50×1.5N50	28.7	4.40	7.39	1.79	2.50	1.62	2.18	1.62
ETF40×60×2.0N30	16.4	1.66	2.65	0.77	1.31	1.14	1.18	1.13
ETF40×60×2.0N60	24.8	2.22	4.00	1.11	1.59	1.15	1.44	1.15
ETF40×60×2.0N60-r	25.1	2.25	4.07	1.12	1.60	1.16	1.44	1.15
ETF50×20×1.5N30	9.9	1.72	2.46	0.68	1.02	1.02	0.92	0.94
ETF60×40×2.0N30	13.2	1.36	2.12	0.65	1.07	1.03	0.98	0.98
ETF60×40×2.0N30-r	13.9	1.43	2.23	0.68	1.13	1.08	1.03	1.03
ETF60×120×3.0N60	44.5	1.83	3.18	0.83	1.33	1.09	1.19	1.08
ETF60×120×3.0N90	56.7	2.15	4.03	1.01	1.45	1.06	1.30	1.05
ETF80×150×3.0N60	24.1	1.19	2.08	0.74	1.24	0.95	1.20	0.97
ETF80×150×3.0N150	44.3	1.75	3.81	1.23	1.62	0.98	1.55	1.00
ETF100×100×3.0N30	25.1	1.17	1.91	0.60	1.11	1.09	1.04	1.04
ETF100×100×3.0N90	42.4	1.66	3.20	0.92	1.29	1.10	1.19	1.05
ETF100×100×3.0N90-r	43.5	1.68	3.26	0.93	1.29	1.10	1.19	1.04
ETF120×60×3.0N30	24.5	1.14	1.73	0.54	0.97	1.04	0.91	0.96
ETF120×60×3.0N60	29.9	1.29	2.13	0.61	0.93	0.96	0.86	0.88
ETF150×80×3.0N30	19.2	1.09	1.65	0.69	1.28	1.19	1.30	1.12
ETF150×80×3.0N90	27.2	1.29	2.34	0.88	1.24	1.12	1.23	1.05
ETF60×60×1.5N30	7.4	1.33	2.05	0.72	1.08	1.07	1.00	0.99
ETF60×60×1.5N60	10.2	1.58	2.84	0.92	1.16	1.02	1.07	0.94
ETF60×60×2.0N30	12.7	1.30	2.10	0.68	1.12	1.05	1.03	1.00
ETF60×60×2.0N60	17.8	1.63	2.95	0.89	1.24	1.02	1.14	0.97
ETF60×60×3.0N30	25.5	1.19	2.02	0.59	1.11	1.02	1.01	1.02
ETF60×60×3.0N60	37.0	1.58	2.93	0.81	1.29	1.03	1.16	1.03
ETF60×60×4.0N30	40.4	1.07	1.89	0.52	1.07	1.04	0.96	1.06
ETF60×60×4.0N60	59.9	1.49	2.80	0.73	1.28	1.09	1.14	1.11
ETF120×120×2.0N60	11.9	1.27	2.02	0.75	1.00	1.10	0.98	0.98
ETF120×120×2.0N120	15.9	1.38	2.71	0.93	1.03	1.00	1.00	0.90
ETF120×120×2.5N60	18.6	1.29	2.11	0.74	1.06	1.08	1.03	1.00
ETF120×120×2.5N120	25.0	1.44	2.83	0.91	1.10	0.99	1.06	0.92
ETF120×120×3.5N60	35.8	1.29	2.19	0.70	1.14	1.06	1.08	1.02
ETF120×120×3.5N120	49.5	1.55	3.03	0.91	1.23	1.01	1.16	0.97
ETF120×120×5.0N60	66.7	1.20	2.11	0.63	1.14	1.01	1.07	1.02
ETF120×120×5.0N120	94.4	1.53	2.99	0.83	1.28	1.00	1.19	1.00
ETF300×300×2.0N150	10.6	1.11	1.79	0.81	0.70	1.06	0.75	0.86
ETF300×300×2.0N300	14.5	1.07	2.47	0.99	0.72	0.98	0.77	0.79

ETF300×300×3.5N150	38.5	1.31	2.36	0.84	0.96	1.19	0.96	1.03
ETF300×300×3.5N300	45.2	1.18	2.77	0.89	0.85	0.95	0.85	0.81
ETF300×300×4.0N150	47.0	1.23	2.25	0.77	0.93	1.10	0.92	0.96
ETF300×300×4.0N300	61.1	1.26	2.93	0.91	0.92	0.97	0.91	0.85
ETF300×300×6.0N150	120.5	1.34	2.65	0.75	1.03	1.10	0.97	0.99
ETF300×300×6.0N300	158.8	1.47	3.49	0.91	1.05	0.99	0.98	0.89
ETF100×80×1.5N40	6.8	1.24	1.88	0.71	0.93	1.11	0.90	0.97
ETF100×80×1.5N80	8.5	1.29	2.36	0.82	0.90	0.98	0.86	0.86
ETF100×80×2.0N40	12.6	1.31	2.09	0.72	1.06	1.15	1.00	1.03
ETF100×80×2.0N80	16.4	1.46	2.71	0.87	1.07	1.05	1.00	0.95
ETF100×80×2.5N40	19.6	1.31	2.16	0.70	1.11	1.13	1.04	1.05
ETF100×80×2.5N80	25.9	1.53	2.86	0.86	1.15	1.06	1.07	0.98
ETF100×80×3.0N40	27.5	1.29	2.18	0.67	1.13	1.10	1.05	1.04
ETF100×80×3.0N80	36.9	1.55	2.93	0.85	1.20	1.06	1.11	1.00
ETF200×150×2.0N75	10.4	1.17	1.77	0.74	0.85	1.14	0.87	0.96
ETF200×150×2.0N150	13.0	1.15	2.20	0.84	0.81	1.01	0.82	0.85
ETF200×150×2.5N75	17.4	1.25	1.97	0.76	0.96	1.19	0.97	1.04
ETF200×150×2.5N150	21.8	1.28	2.47	0.87	0.93	1.06	0.92	0.92
ETF200×150×4.0N75	46.5	1.32	2.23	0.74	1.14	1.20	1.10	1.10
ETF200×150×4.0N150	59.1	1.45	2.83	0.88	1.12	1.09	1.08	1.00
ETF200×150×4.5N75	63.1	1.31	2.37	0.71	1.10	1.16	1.03	1.06
ETF200×150×4.5N150	82.1	1.50	3.08	0.86	1.12	1.08	1.04	0.98
ETF400×200×3.0N100	20.9	1.21	1.70	0.75	0.83	1.22	0.88	1.00
ETF400×200×3.0N200	24.2	1.12	1.97	0.79	0.73	1.07	0.77	0.87
ETF400×200×4.0N100	41.0	1.27	1.96	0.76	0.97	1.30	1.00	1.10
ETF400×200×4.0N200	48.1	1.24	2.30	0.83	0.88	1.16	0.90	0.98
ETF400×200×6.0N100	105.3	1.31	2.32	0.72	1.07	1.28	1.03	1.12
ETF400×200×6.0N200	125.0	1.36	2.75	0.80	0.99	1.16	0.95	1.01
ETF400×200×8.0N100	188.8	1.31	2.42	0.70	1.15	1.27	1.09	1.14
ETF400×200×8.0N200	226.3	1.41	2.90	0.79	1.09	1.16	1.03	1.05
Mean		1.46	2.62	0.82	1.13	1.10	1.07	1.01
COV		0.331	0.328	0.224	0.240	0.075	0.204	0.078
Resistance factor, ϕ		0.70	0.91	0.90	0.80	0.85	0.80	0.85
Reliability index, β		3.04	3.74	1.27	2.52	3.07	2.54	2.75

Table 9: Comparison of test and FE strengths with design predicted strengths for EL condition

Specimen	P_u (P_t or P_{FEA})	P_u/P_{ASCE}	P_u/P_{ASCE}	P_u/P_{EC}	P_u/P_{NAS}	P_u/P_{NAS}	$P_u/P_{Z\&Y}$	$P_u/P_{L\&Y}$	P_u/P_1	P_u/P_2
	(kN)	EOF[#]	ETF[*]		EOF[#]	ETF[*]				
EL20×50×1.5N30	20.7	2.52	3.43	5.24	1.63	1.37	1.71	1.50	1.41	1.32
EL20×50×1.5N50	29.3	3.15	4.30	7.20	1.90	1.73	2.03	1.36	1.53	1.18
EL40×60×2.0N30	19.9	1.45	1.98	3.14	1.09	0.89	1.09	1.14	0.98	0.97
EL40×60×2.0N60	29.6	1.92	2.63	4.71	1.32	1.25	1.40	1.11	1.15	0.94
EL50×20×2.0N30	12.1	1.50	2.08	3.02	0.99	0.88	0.98	1.15	0.89	0.92
EL60×40×2.0N30	17.6	1.29	1.78	2.74	0.97	0.81	0.95	1.11	0.88	0.90
EL60×40×2.0N50	22.0	1.46	2.01	3.37	1.03	0.96	1.05	1.06	0.92	0.86
EL60×120×3.0N60	51.9	1.55	2.13	3.69	1.10	0.96	1.14	1.09	1.01	0.94
EL60×120×3.0N120	74.7	1.90	2.60	5.29	1.26	1.29	1.39	0.98	1.13	0.85
EL80×150×3.0N60	33.2	1.16	1.59	2.84	0.95	0.98	1.08	1.09	1.14	0.97
EL80×150×3.0N150	49.9	1.41	1.93	4.27	1.06	1.35	1.29	0.92	1.23	0.82
EL100×100×3.0N30	33.3	1.14	1.57	2.54	0.99	0.82	0.98	1.29	1.04	1.06
EL100×100×3.0N90	48.2	1.42	1.95	3.67	1.04	1.10	1.14	1.14	1.06	0.94
EL100×100×3.0N90-	47.8	1.37	1.89	3.63	1.03	1.05	1.09	1.09	0.99	0.89
EL120×60×3.0N30	31.4	1.04	1.44	2.20	0.83	0.68	0.79	1.13	0.83	0.90
EL120×60×3.0N60	38.7	1.21	1.67	2.76	0.86	0.81	0.87	1.10	0.83	0.87
EL120×60×3.0N60-r	36.6	1.13	1.57	2.59	0.80	0.74	0.80	1.01	0.76	0.80
EL150×80×3.0N30	24.8	0.97	1.35	2.11	0.90	0.85	0.91	1.30	1.13	1.04
EL150×80×3.0N90	32.5	1.10	1.53	2.79	0.86	1.04	0.96	1.16	1.05	0.93
EL150×80×3.0N90-r	33.2	1.12	1.57	2.85	0.88	1.06	0.99	1.18	1.07	0.95
EL60×60×1.5N30	10.7	1.39	1.92	2.96	1.10	1.04	1.11	1.34	1.06	1.07
EL60×60×1.5N60	13.8	1.53	2.12	3.82	1.13	1.24	1.20	1.18	1.05	0.94
EL60×60×2.0N30	18.4	1.37	1.89	3.04	1.13	0.98	1.14	1.32	1.09	1.09
EL60×60×2.0N60	24.1	1.59	2.19	3.99	1.20	1.21	1.28	1.20	1.12	0.98
EL60×60×3.0N30	36.4	1.24	1.70	2.88	1.09	0.84	1.08	1.26	1.06	1.09
EL60×60×3.0N60	49.1	1.53	2.10	3.89	1.21	1.08	1.27	1.18	1.13	1.02
EL60×60×4.0N30	57.8	1.12	1.53	2.70	1.03	0.74	1.02	1.27	1.00	1.13
EL60×60×4.0N60	78.2	1.42	1.94	3.65	1.16	0.96	1.21	1.21	1.09	1.08
EL120×120×2.0N60	14.7	1.11	1.56	2.50	0.80	0.93	0.85	1.16	0.88	0.91
EL120×120×2.0N120	19.7	1.21	1.70	3.34	0.84	1.14	0.94	1.05	0.90	0.83
EL120×120×2.5N60	23.4	1.16	1.62	2.65	0.86	0.93	0.91	1.18	0.94	0.94
EL120×120×2.5N120	30.9	1.28	1.79	3.50	0.90	1.13	1.01	1.06	0.95	0.85
EL120×120×3.5N60	46.4	1.21	1.67	2.84	0.94	0.91	0.99	1.20	1.02	0.99
EL120×120×3.5N120	61.0	1.39	1.91	3.74	0.99	1.12	1.11	1.09	1.05	0.90
EL120×120×5.0N60	87.2	1.14	1.57	2.76	0.94	0.82	0.98	1.14	1.02	0.99
EL120×120×5.0N120	114.4	1.35	1.86	3.62	1.00	1.01	1.11	1.05	1.06	0.91
EL300×300×2.0N150	13.1	0.90	1.37	2.22	0.58	1.00	0.59	1.03	0.68	0.79

EL300×300×2.0N300	17.1	0.82	1.25	2.90	0.58	1.16	0.61	0.91	0.66	0.70
EL300×300×3.5N150	50.3	1.19	1.71	3.08	0.82	1.10	0.86	1.30	0.92	1.00
EL300×300×3.5N300	68.6	1.25	1.79	4.20	0.87	1.36	0.96	1.20	0.95	0.93
EL300×300×4.0N150	68.4	1.26	1.79	3.28	0.89	1.12	0.93	1.35	0.98	1.05
EL300×300×4.0N300	86.9	1.26	1.79	4.16	0.88	1.29	0.97	1.16	0.94	0.90
EL300×300×6.0N150	156.2	1.24	1.73	3.44	0.95	0.97	0.96	1.22	0.92	0.96
EL300×300×6.0N300	232.3	1.54	2.15	5.11	1.12	1.33	1.20	1.24	1.05	0.97
EL100×80×1.5N40	8.7	1.14	1.60	2.43	0.86	0.92	0.85	1.21	0.84	0.94
EL100×80×1.5N80	13.7	1.46	2.07	3.79	1.06	1.32	1.11	1.32	1.01	1.03
EL100×80×2.0N40	19.8	1.47	2.05	3.27	1.16	1.13	1.15	1.54	1.14	1.21
EL100×80×2.0N80	26.2	1.67	2.33	4.33	1.23	1.39	1.29	1.44	1.16	1.13
EL100×80×2.5N40	30.1	1.45	2.02	3.32	1.19	1.07	1.18	1.51	1.16	1.20
EL100×80×2.5N80	40.2	1.71	2.37	4.44	1.28	1.34	1.34	1.43	1.21	1.14
EL100×80×3.0N40	41.4	1.41	1.94	3.28	1.18	1.01	1.17	1.45	1.15	1.18
EL100×80×3.0N80	55.6	1.69	2.33	4.40	1.29	1.27	1.35	1.39	1.21	1.12
EL200×150×2.0N75	15.3	1.20	1.73	2.60	0.82	1.09	0.84	1.38	0.93	1.06
EL200×150×2.0N150	19.9	1.22	1.76	3.38	0.83	1.29	0.89	1.27	0.92	0.98
EL200×150×2.5N75	25.3	1.28	1.82	2.86	0.91	1.10	0.93	1.45	1.02	1.12
EL200×150×2.5N150	33.0	1.35	1.93	3.74	0.93	1.32	1.01	1.34	1.02	1.04
EL200×150×4.0N75	64.9	1.32	1.84	3.11	1.01	1.03	1.04	1.44	1.12	1.15
EL200×150×4.0N150	85.7	1.50	2.10	4.10	1.07	1.27	1.17	1.37	1.15	1.09
EL200×150×4.5N75	90.4	1.35	1.88	3.39	1.10	1.01	1.08	1.43	1.08	1.13
EL200×150×4.5N150	120.2	1.58	2.19	4.52	1.18	1.26	1.23	1.36	1.11	1.08
EL400×200×3.0N100	28.5	1.10	1.64	2.31	0.73	1.02	0.71	1.32	0.87	1.01
EL400×200×3.0N200	33.1	1.02	1.53	2.69	0.67	1.08	0.68	1.16	0.77	0.89
EL400×200×4.0N100	56.0	1.20	1.74	2.68	0.86	1.04	0.85	1.46	1.00	1.12
EL400×200×4.0N200	64.4	1.15	1.67	3.08	0.78	1.11	0.81	1.27	0.88	0.98
EL400×200×6.0N100	143.1	1.26	1.78	3.15	1.01	0.98	0.97	1.47	1.02	1.14
EL400×200×6.0N200	161.8	1.25	1.76	3.56	0.92	1.04	0.93	1.26	0.90	0.98
EL400×200×8.0N100	246.4	1.22	1.71	3.16	1.04	0.91	0.99	1.42	1.04	1.12
EL400×200×8.0N200	287.8	1.29	1.79	3.69	0.99	1.00	1.00	1.27	0.95	1.00
Mean		1.36	1.90	3.41	1.01	1.07	1.05	1.24	1.02	1.00
COV		0.247	0.235	0.254	0.208	0.178	0.217	0.115	0.144	0.112
Resistance factor, ϕ		0.70	0.70	0.91	0.80	0.90	0.80	0.85	0.80	0.85
Reliability index, β		3.40	4.48	5.11	2.33	2.31	2.42	3.35	2.70	2.56

Note: "#" means using EOF design equation; "*" means using ETF design equation.

Table 10: Coefficients for unified design equation

Provision	Material	Section type	Load condition	Coefficients					Limits ($\theta = 90^{\circ}$)			
				C	C_R	C_N	C_h	ϕ	r_i/t	N/t	h/t	N/h
NAS (2016)	Carbon steel	Single web channel	EOF	4.0	0.14	0.35	0.02	0.80	≤ 5.0	≤ 210	≤ 200	≤ 2.0
			ETF	13.0	0.32	0.05	0.04	0.90	≤ 3.0	≤ 210	≤ 200	≤ 2.0
Zhou & Young (2008)	Duplex stainless steel	Square and rectangular hollow sections	EOF	5.0	0.40	0.50	0.020	0.70	≤ 2.0	≤ 50	≤ 50	≤ 2.0
			ETF	3.0	0.36	0.50	0.020	0.80	≤ 2.0	≤ 50	≤ 50	≤ 2.0
			EL	5.8	0.26	0.18	0.001	0.80	≤ 2.0	≤ 50	≤ 200	≤ 1.6
Proposed	Lean duplex stainless steel		EOF	5.0	0.40	0.55	0.032	0.85	≤ 2.0	≤ 150	≤ 145	≤ 1.5
			ETF	3.5	0.40	0.55	0.032	0.80	≤ 2.0	≤ 150	≤ 145	≤ 1.5
			EL	4.8	0.40	0.55	0.032	0.80	≤ 2.0	≤ 150	≤ 145	≤ 1.5

Note: The table is suitable to stiffened or partially stiffened flanges that unfastened to support.

Table 11: Coefficients for modified direct strength method

Provision	Load condition	a	b	n	λ_k	γ	ϕ
Li & Young (2017; 2018)	EOF	0.96	0.23	0.51	0.584	1.00	0.85
	ETF	0.66	0.17	0.55	0.447	0.94	0.85
	EL	0.69	0.09	0.49	0.543	1.05	0.85
Proposed	EOF	0.98	0.20	0.50	0.700	1.00	0.85
	ETF	0.71	0.20	0.50	0.500	0.85	0.85
	EL	0.95	0.20	0.50	0.600	1.05	0.85

Note: The table is suitable to stiffened or partially stiffened flanges that unfastened to support.
The proposed coefficients apply when $10 \le h/t \le 145$, $r_i/t \le 2.0$, $N/t \le 150$ and $N/h \le 1.5$.

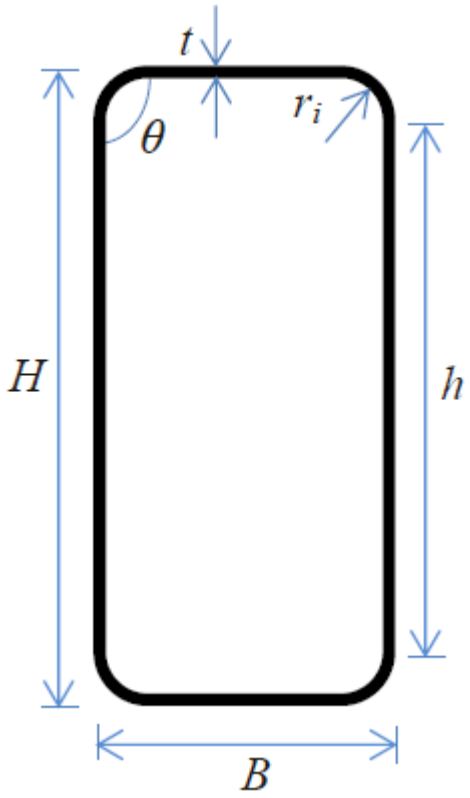

Figure 1: Definition of symbols in a tubular section

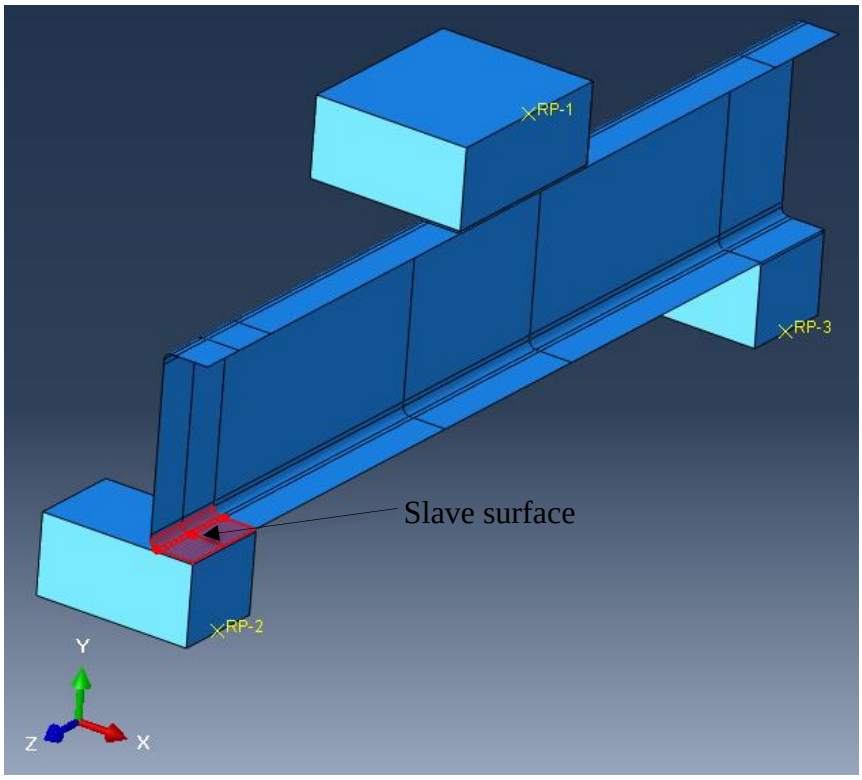

Figure 2: Symmetric finite element model (FEM) for specimen under EOF loading condition (a) Definition of slave surface at flange and corner regions

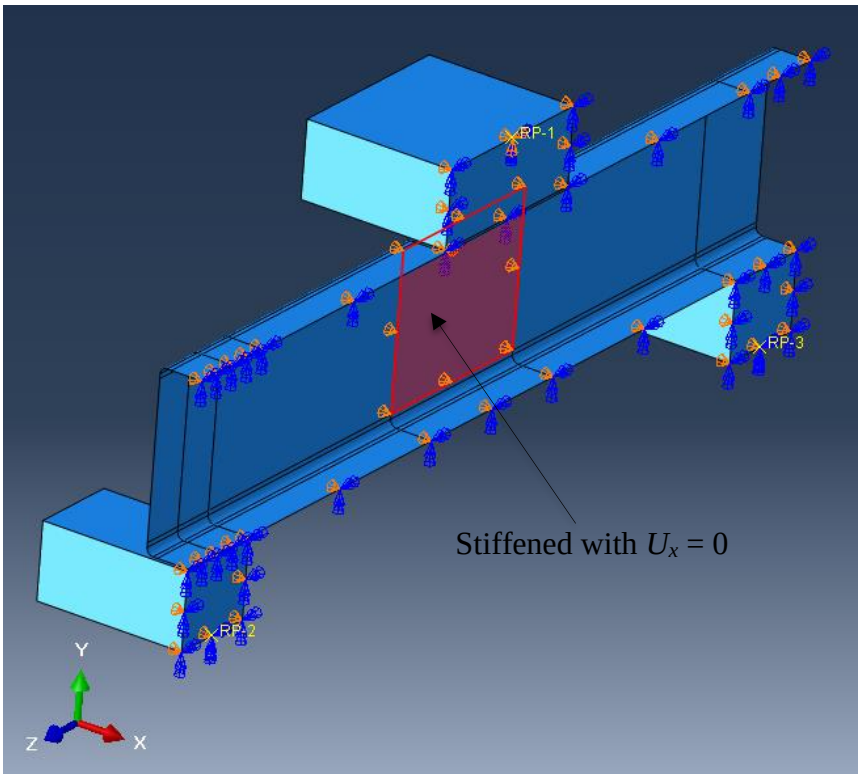

Figure 2: Symmetric finite element model (FEM) for specimen under EOF loading condition (b) Definition of the stiffened web

Figure 3: Comparison of test and FEM for Specimen EOF120×60×3.0N60 (a) Specimen in the test

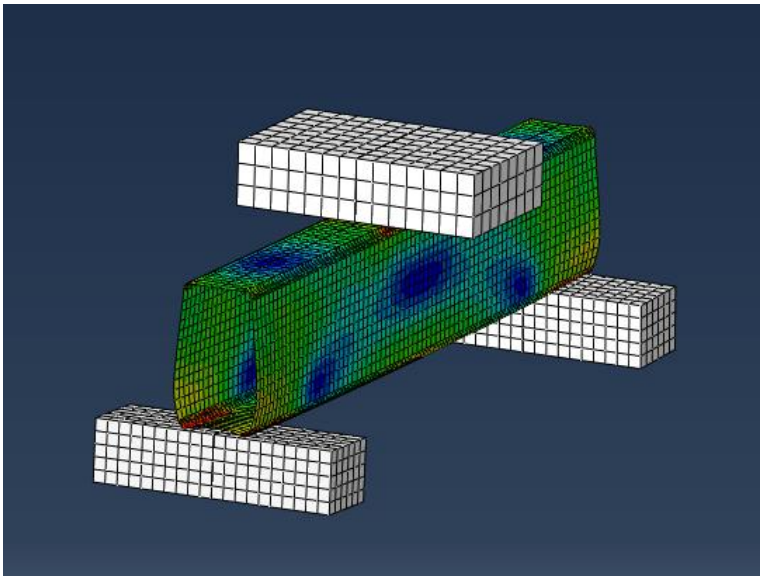

Figure 3: Comparison of test and FEM for Specimen EOF120×60×3.0N60 (b) Specimen in FEM

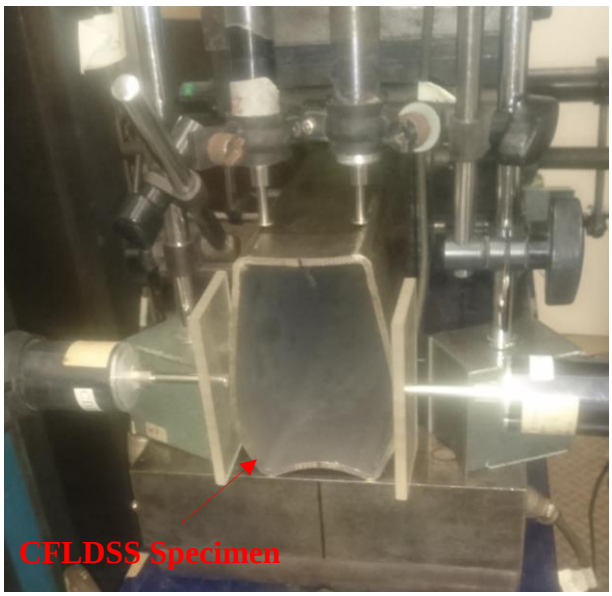

Figure 4: Web crippling failure of Specimen EOF120×60×3.0N60 (a) Failure at specimen end in test

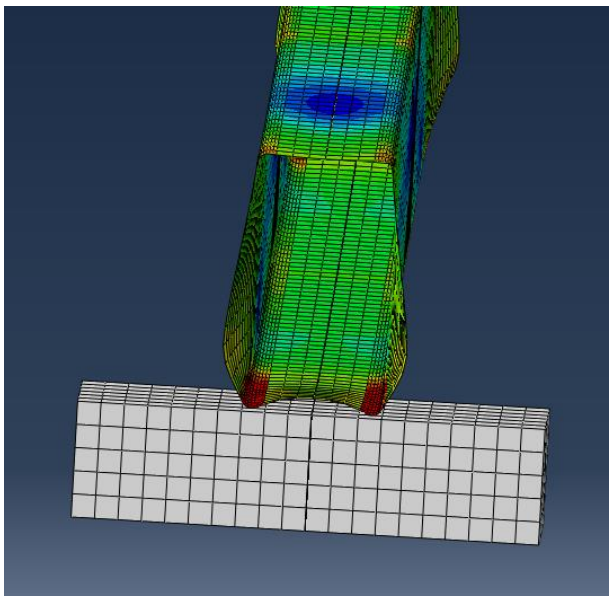

Figure 4: Web crippling failure of Specimen EOF120×60×3.0N60 (b) Failure at specimen end in FEM

Figure 5: Comparison of test and FEM for Specimen ETF100×100×3.0N90 (a) Specimen in the test

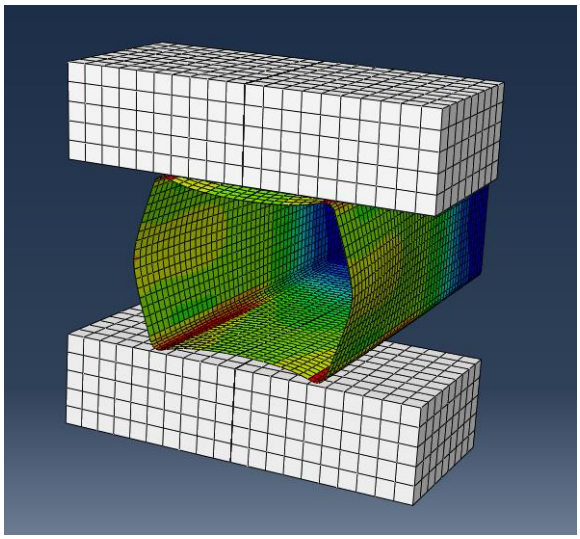

Figure 5: Comparison of test and FEM for Specimen ETF100×100×3.0N90 (b) 3-D view of specimen in FEM

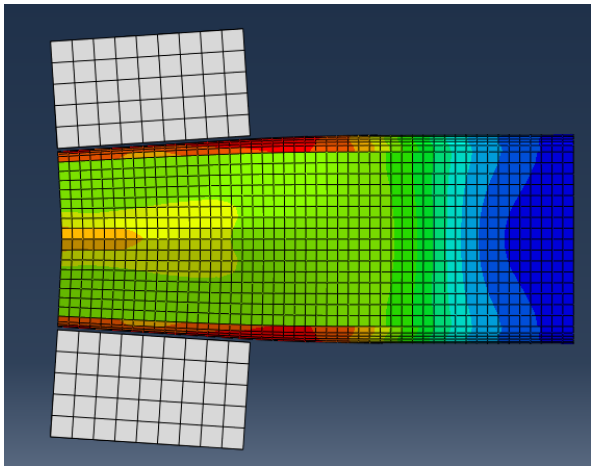

Figure 5: Comparison of test and FEM for Specimen ETF100×100×3.0N90 (c) Side view of specimen in FEM

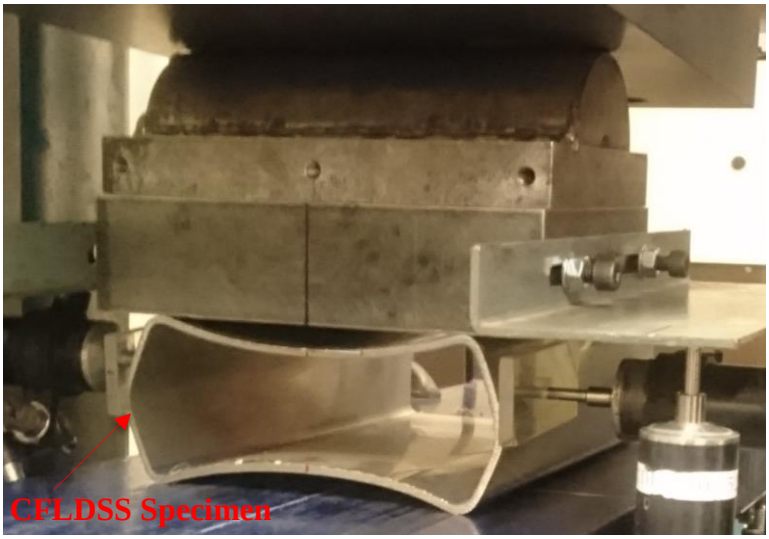

Figure 6: Comparison of test and FEM for Specimen EL80×150×3.0N150 (a) Specimen in the test

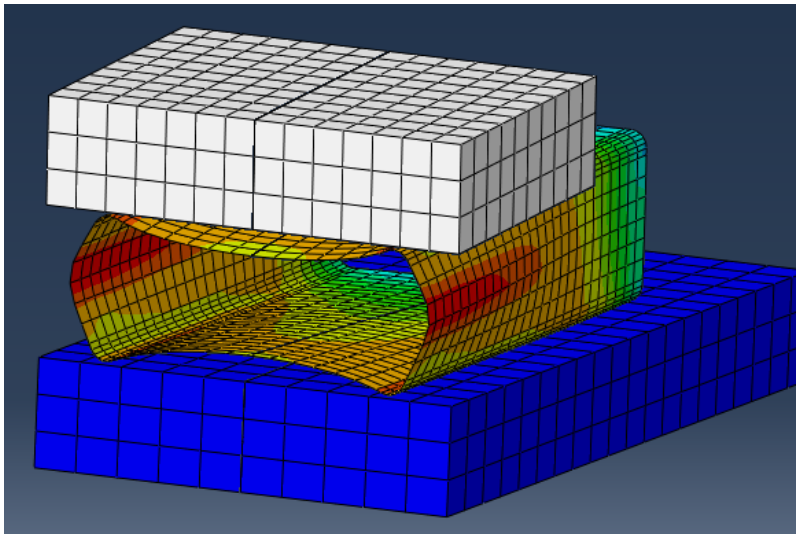

Figure 6: Comparison of test and FEM for Specimen EL80×150×3.0N150 (b) 3-D view of specimen in FEM

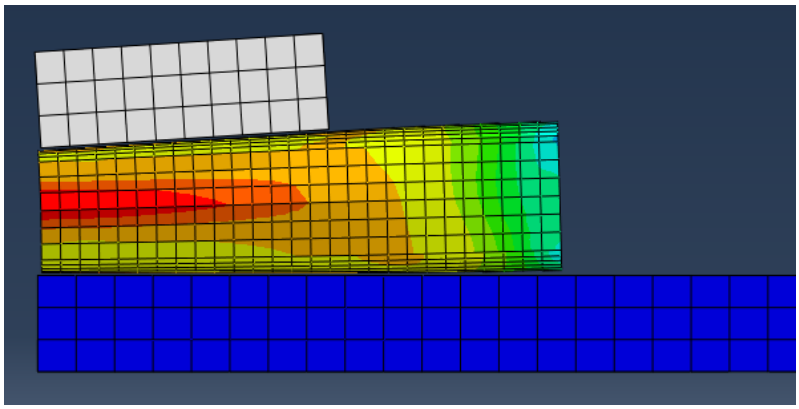

Figure 6: Comparison of test and FEM for Specimen EL80×150×3.0N150 (c) Side view of specimen in FEM

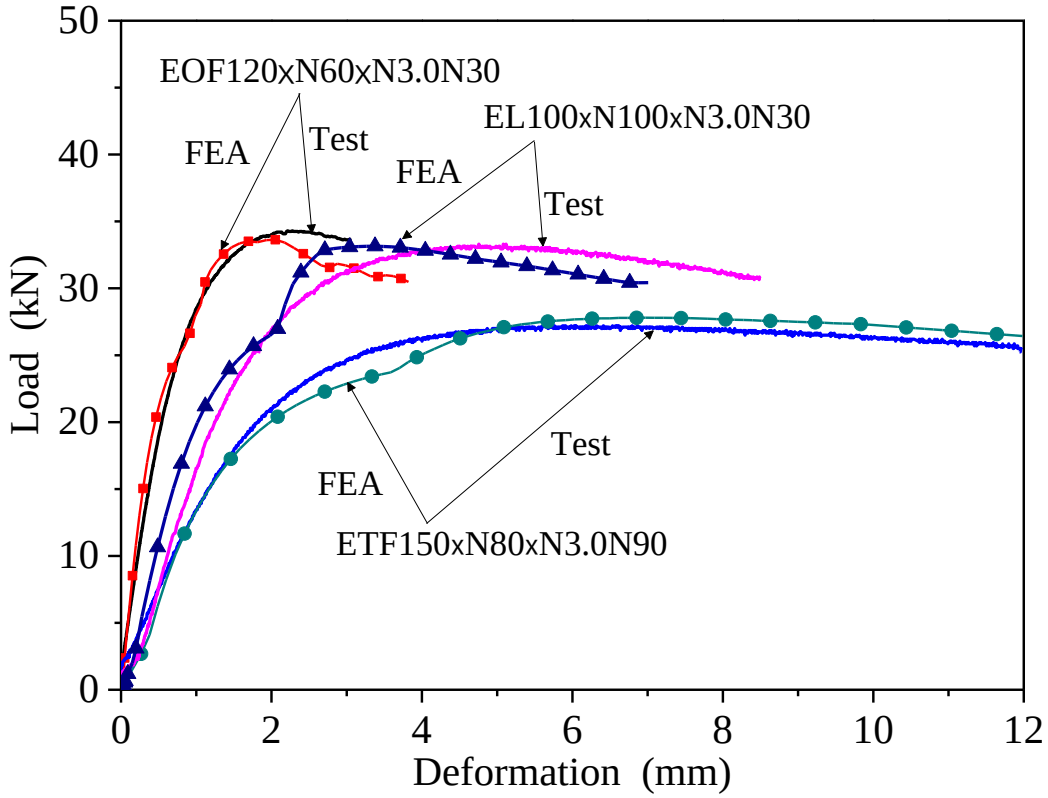

Figure 7: Comparison of load-deformation curves obtained from tests and finite element analyses

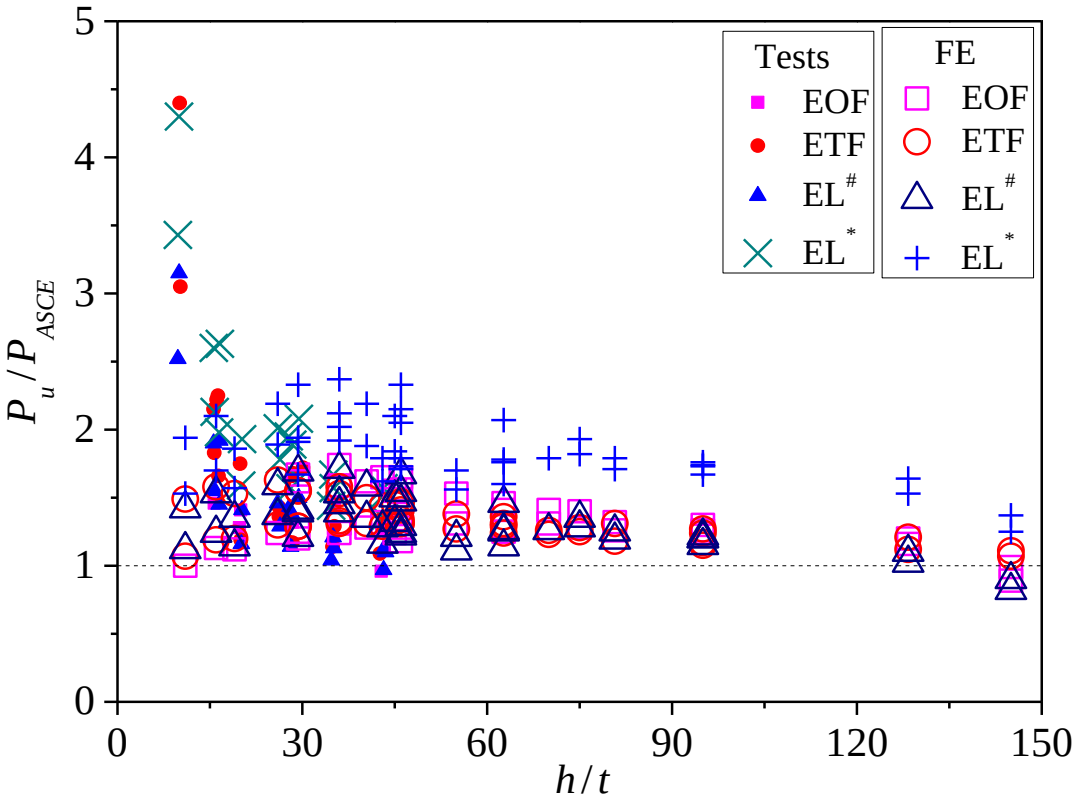

Figure 8: Comparison of test and FE results with ASCE predictions (2002)

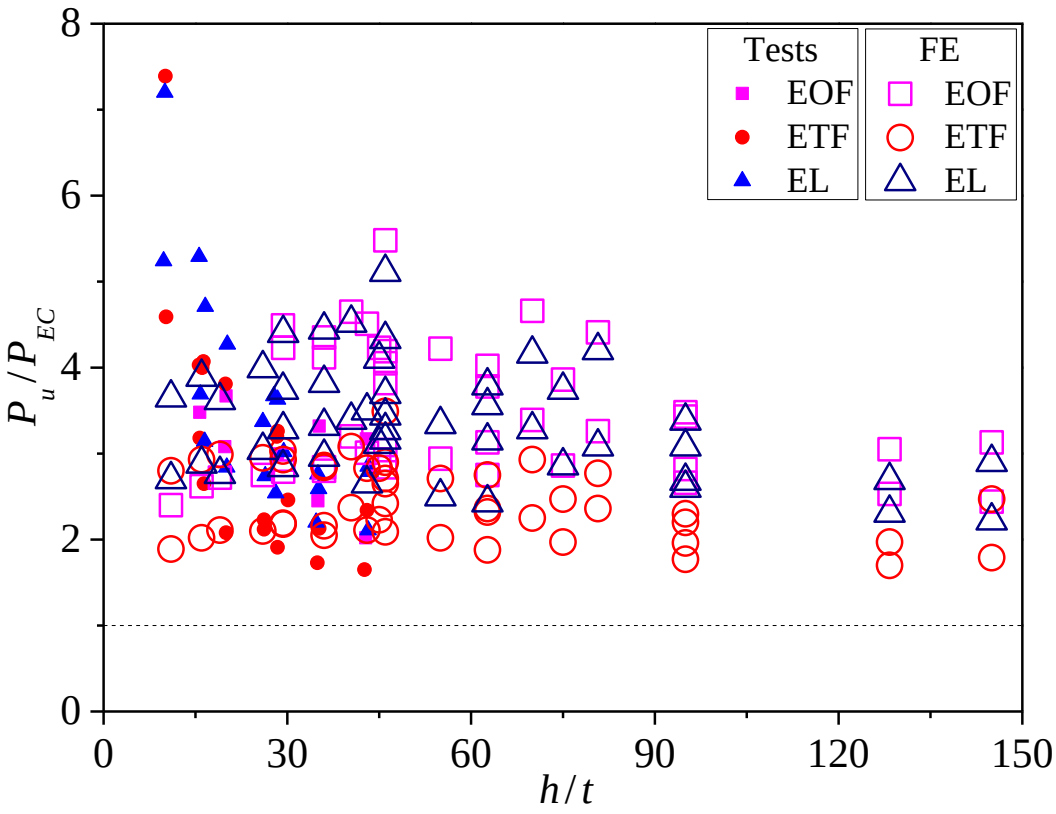

Figure 9: Comparison of test and FE results with EC3-1.3 predictions (2006)

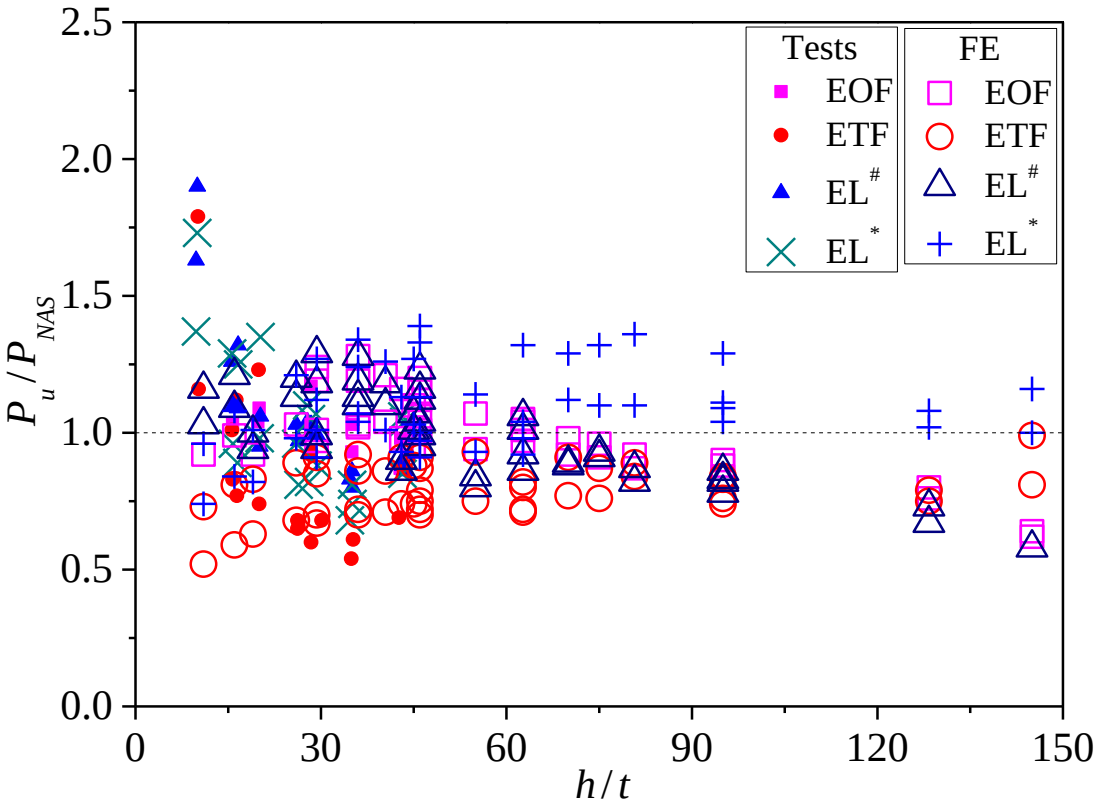

Figure 10: Comparison of test and FE results with NAS predictions (2016)

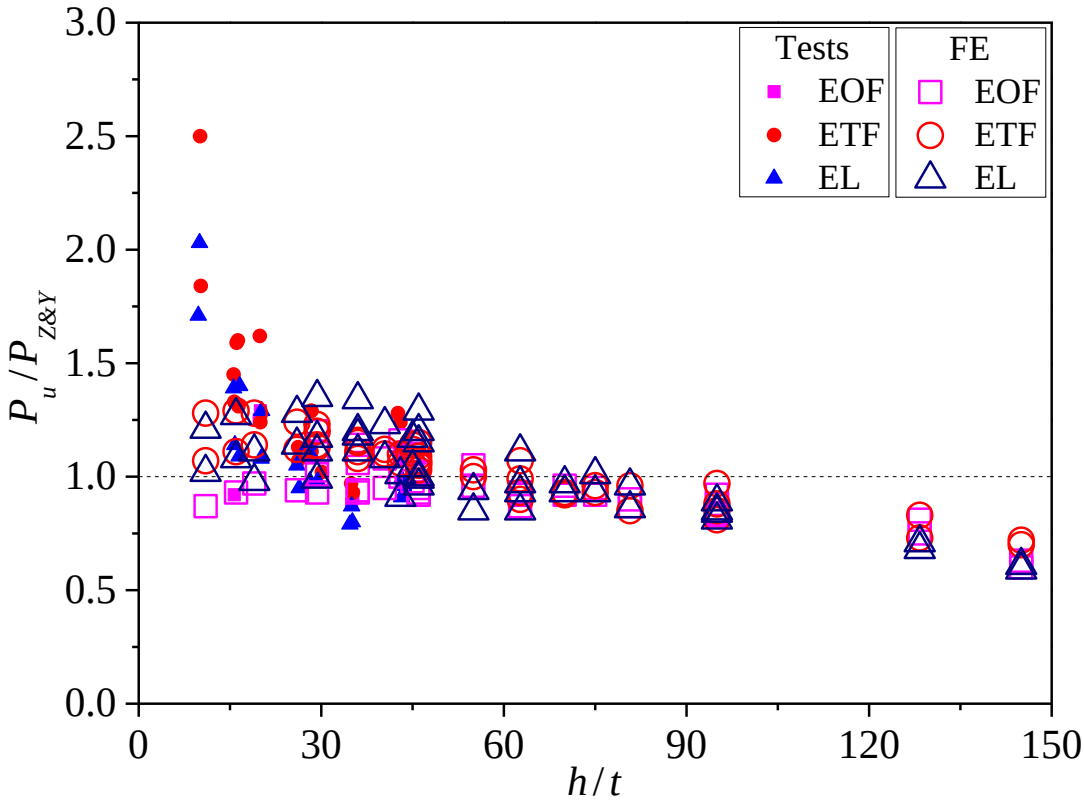

Figure 11: Comparison of test and FE results with predictions by Zhou and Young (2008)

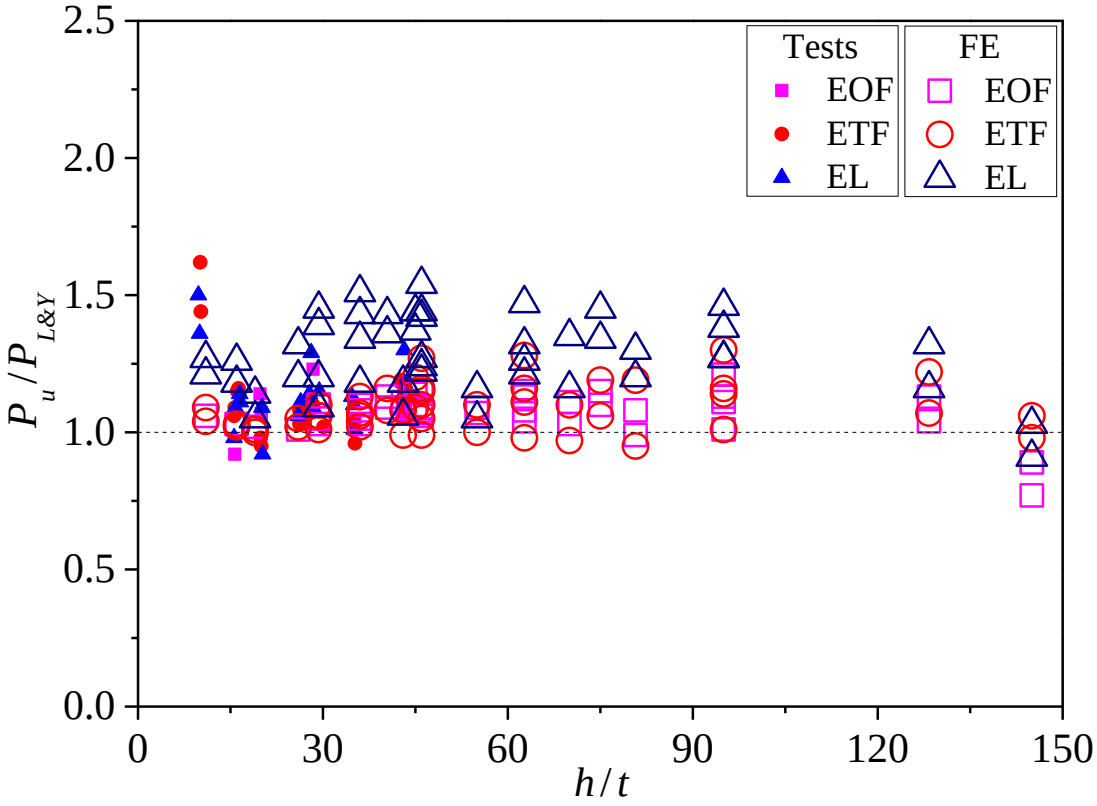

Figure 12: Comparison of test and FE results with predictions by Li and Young (2017; 2018)

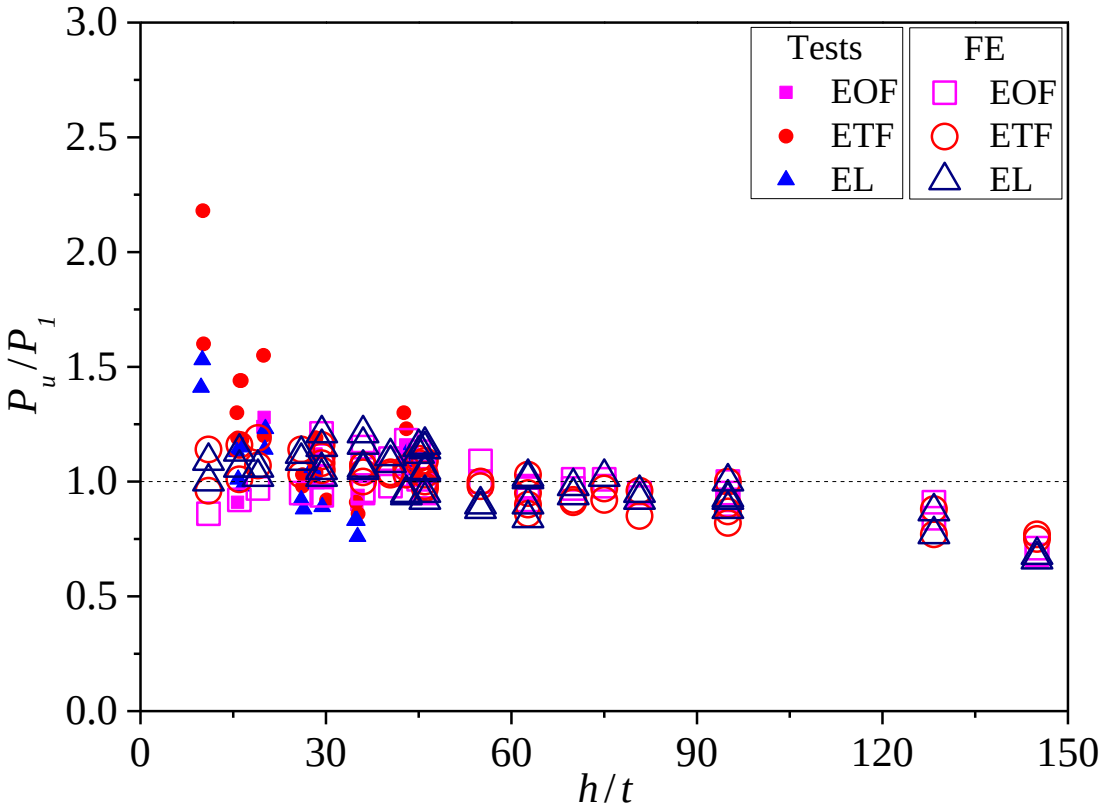

Figure 13: Comparison of test and FE results with predictions by NAS (2016) using proposed coefficients

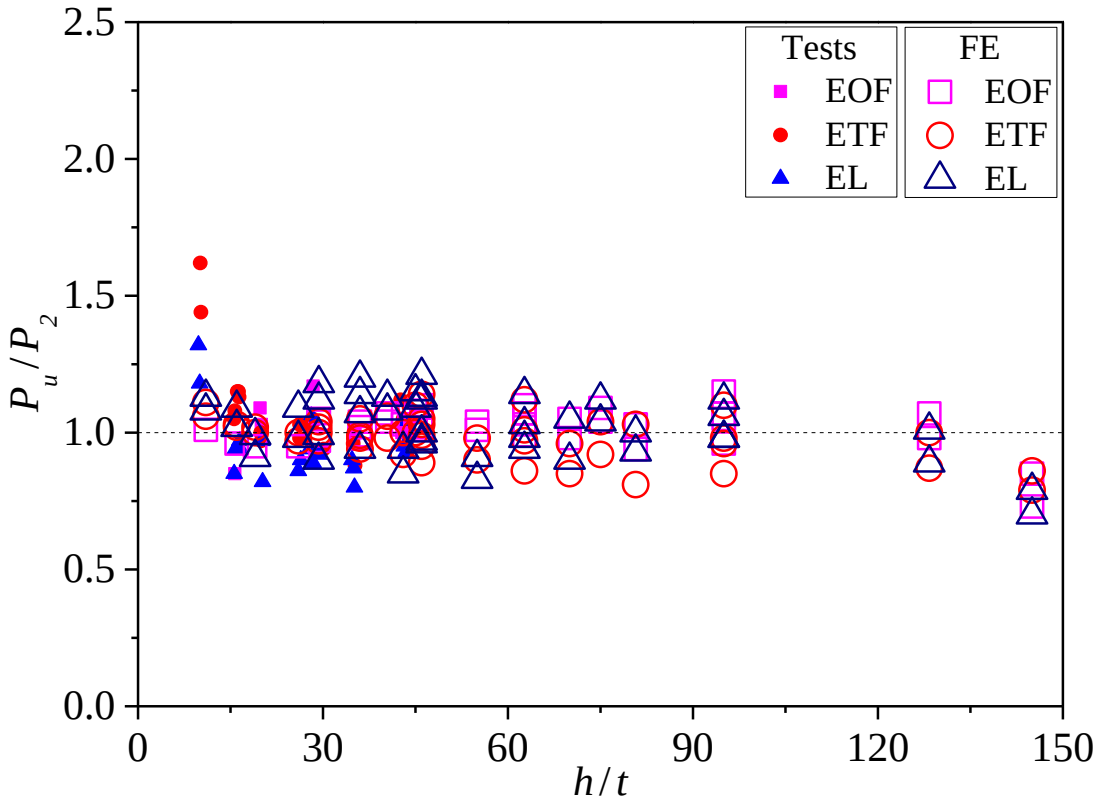

Figure 14: Comparison of test and FE results with predictions by modified DSM using proposed coefficients

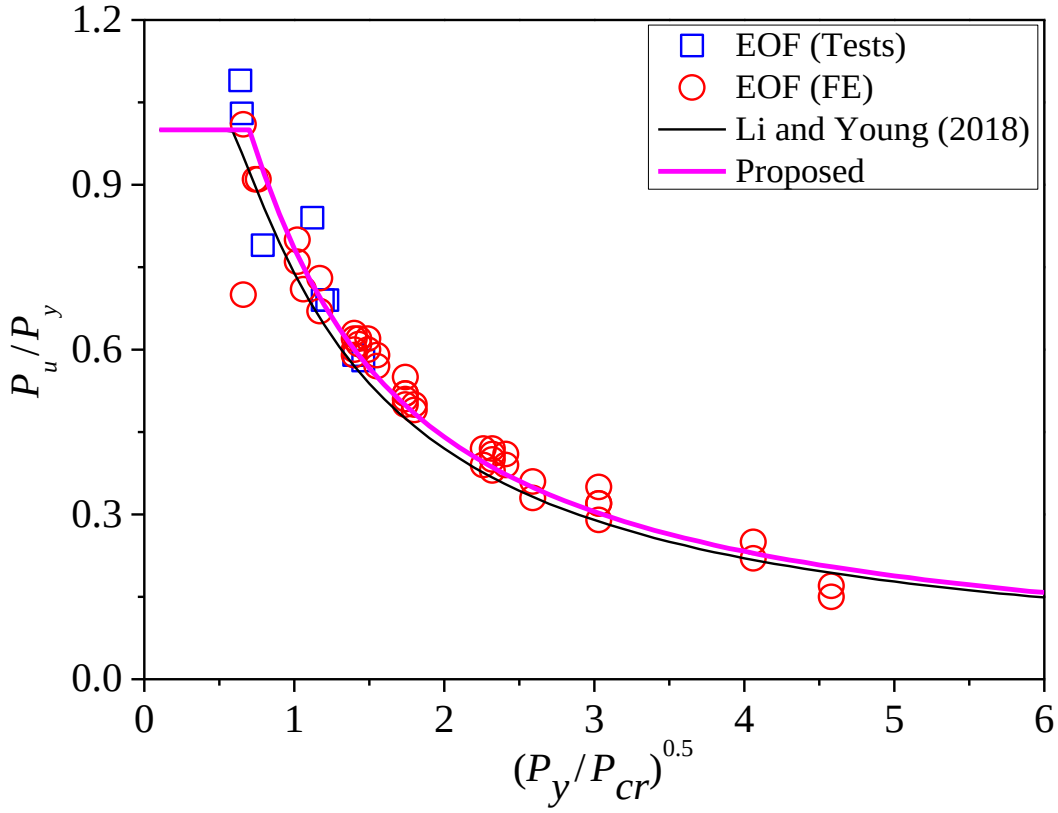

Figure 15: Comparison of test and FE results with DSM curves for EOF condition

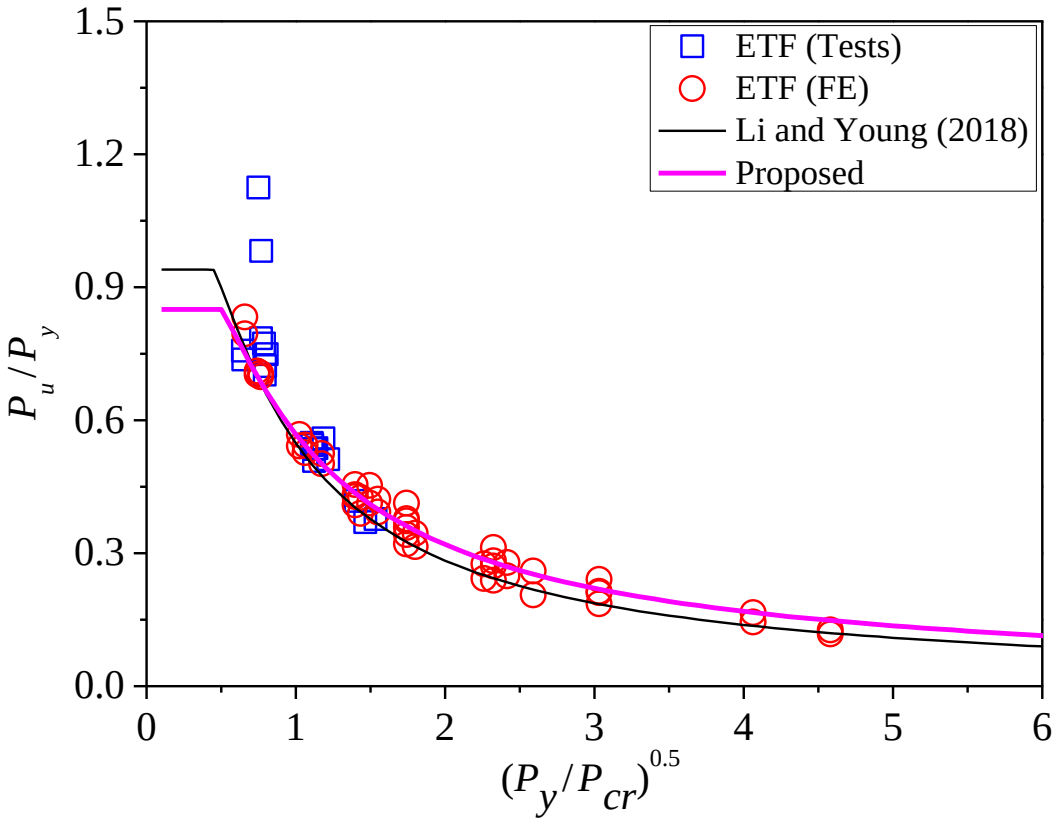

Figure 16: Comparison of test and FE results with DSM curves for ETF condition

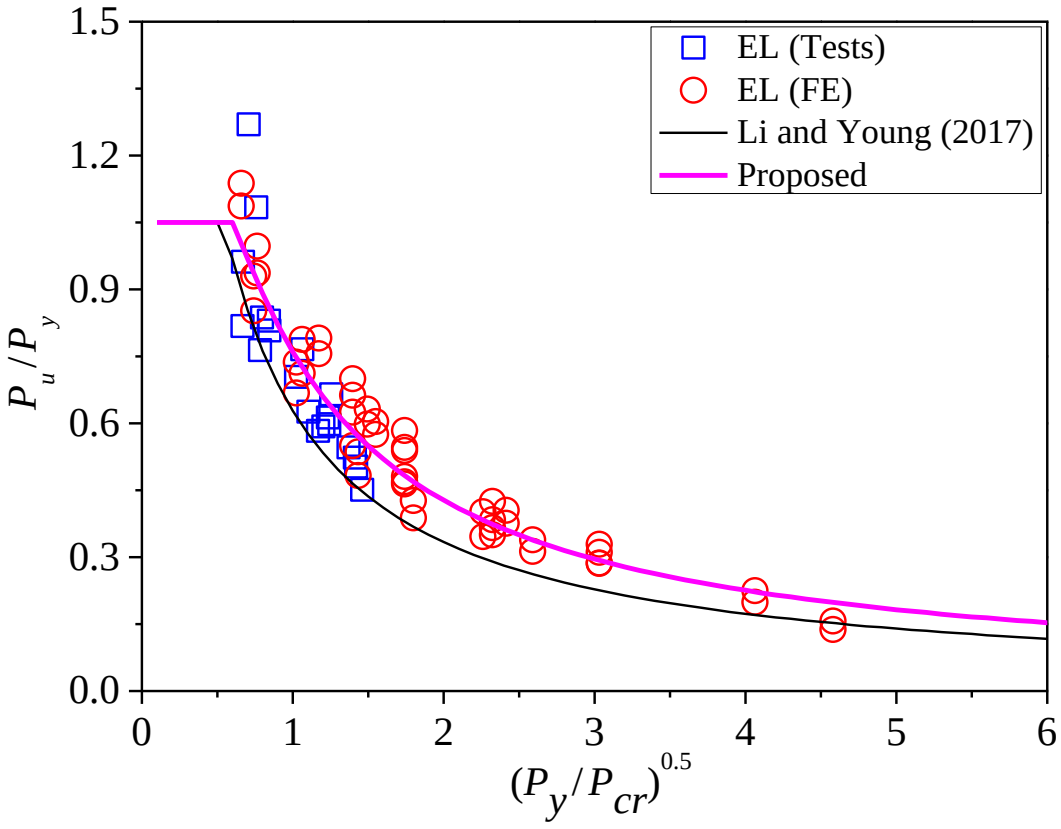

Figure 17: Comparison of test and FE results with DSM curves for EL condition